Evidence of fire in the Pliocene Arctic in response to elevated CO_2 and temperature

Tamara Fletcher[1*], Lisa Warden[2*], Jaap S. Sinninghe Damsté[2,3], Kendrick J. Brown[4,5], Natalia Rybczynski[6,7], John Gosse[8], and Ashley P Ballantyne[1]

[1] College of Forestry and Conservation, University of Montana, Missoula, 59812, USA
[2] Department of Marine Microbiology and Biogeochemistry, NIOZ Royal Netherlands Institute for Sea Research, Den Berg, 1790, Netherlands
[3] Department of Earth Sciences, University of Utrecht, Utrecht, 3508, Netherlands
[4] Natural Resources Canada, Canadian Forest Service, Victoria, V8Z 1M, Canada
[5] Department of Earth, Environmental and Geographic Science, University of British Columbia Okanagan, Kelowna, V1V 1V7, Canada
[6] Department of Palaeobiology, Canadian Museum of Nature, Ottawa, K1P 6P4, Canada
[7] Department of Biology & Department of Earth Sciences, Carleton University, Ottawa, K1S 5B6, Canada
[8] Department of Earth Sciences, Dalhousie University, Halifax, B3H 4R2, Canada
*Authors contributed equally to this work

Correspondence to: Tamara Fletcher (tamara.fletcher@umontana.edu)

Abstract. The mid-Pliocene is a valuable time interval for understanding the mechanisms that determine equilibrium climate at current atmospheric CO_2 concentrations. One intriguing, but not fully understood, feature of the early to mid-Pliocene climate is the amplified arctic temperature response. Current models underestimate the degree of warming in the Pliocene Arctic and validation of proposed feedbacks is limited by scarce terrestrial records of climate and environment, as well as discrepancies in current CO_2 proxy reconstructions. Here we reconstruct the CO_2, summer temperature and fire regime from a sub-fossil fen-peat deposit on west-central Ellesmere Island, Canada, that has been chronologically constrained using radionuclide dating to 3.9 +1.5/-0.5 Ma.

An empirical transfer function was derived and applied to carbon isotopic measurements of paleo mosses to yield an estimate of Pliocene mean atmospheric CO_2 concentrations of 410 ± 50 ppm, which are slightly lower than theoretical model predictions of 510 ppm. The estimate for average mean summer temperature is 15.4±0.8°C using specific bacterial membrane lipids, i.e. branched glycerol dialkyl glycerol tetraethers. Macro-charcoal was present in all samples from this Pliocene section with notably higher charcoal concentration in the upper part of the sequence. This change in charcoal was synchronous with a change in vegetation that saw fire promoting taxa increase in abundance. Paleovegetation reconstructions are consistent with warm summer temperatures, relatively low summer precipitation and an incidence of fire comparable to fire adapted boreal forests of North America, or potentially central Siberia.

To our knowledge, this study represents the northern-most evidence of fire during the Pliocene and highlights the important role of forest fire in the ecology and climatic processes of the Pliocene High Arctic. The results provide evidence that terrestrial fossil localities in the Pliocene High Arctic were probably formed during warm intervals that coincided with relatively high CO_2 concentrations that supported productive biotic communities. This study indicates that interactions between paleovegetation and paleoclimate were mediated by fire in the High Arctic during the Pliocene, even though CO_2 concentrations were similar to modern.

1 Introduction

Current rates of warming in the Arctic are almost double the rate of global warming. Since 1850, global land surface temperatures have increased by approximately 1.0°C, whereas arctic land surface temperatures have increased by 2.0°C (Jones and Moberg, 2003; Pagani et al., 2010, Francis and Skific, 2015). Such arctic amplification of temperatures has also occurred during other warm climate anomalies in Earth's past. Paleoclimate records from the Arctic indicate that the change in arctic summer temperatures during past global warm periods was 3–4 times larger than global temperature change (Miller et al., 2010). While the latest ensemble of earth system models (ESMs) provide fairly accurate predictions of the modern amplification of arctic temperatures hitherto observed (Marshall et al., 2014), they often under-predict the amplification of arctic temperatures during past warm intervals in Earth's history, including the Eocene (33.9–56 Ma; Huber, 2008; Shellito et al., 2009), and the Pliocene (2.6–5.3 Ma; Dowsett et al., 2012; Salzmann et al., 2013) epochs. These differences suggest that either the models are not simulating the full array of feedback mechanisms properly for past climates, or that the full array of fast and slow feedback mechanisms have not fully engaged for the modern Arctic. If the later, the Arctic region has yet to reach the full amplification potential demonstrated in the past.

The Pliocene is an intriguing climatic interval that may offer important insights into climate feedbacks. Atmospheric CO_2 values varied (Royer et al., 2007) decreasing from values comparable to modern (Haywood et al., 2016; Pagani et al., 2010; Stap et al., 2016), to lower levels (Raymo et al., 2006); a state transition that may revert in the future under high CO_2. Of additional importance, continental configurations were similar to present (Dowsett et al., 2016). While global mean annual temperatures (MATs) during the Pliocene were only ~ 3°C warmer than present day (Fig. 1), arctic land surface MATs may have been as much as 15 to 20°C warmer (Ballantyne et al., 2010; Csank et al., 2011a; Csank et al., 2011b; Fletcher et al., 2017). Further, arctic sea surface temperatures may have been as much as 10 to 15°C warmer than modern (Robinson, 2009), and sea-levels were approximately 25m higher than present (Dowsett et al., 2016). As such, the terrestrial environment of the Arctic was significantly different, with tree line ecosystems at much higher latitudes nearly eliminating the tundra biome (Salzmann et al., 2008).

Several mechanisms have been proposed as drivers of arctic amplification, including vastly reduced sea-ice extent (Ballantyne et al., 2013), cloud and atmospheric water vapor effects (e.g. Feng et al., 2016; Swann et al., 2010), vegetation controls on albedo (Otto-Bliesner and Upchurch Jr, 1997), and increased meridional heat transport by the oceans (Dowsett et al., 1992) though it is now considered to be of lesser influence (Hwang et al., 2011). We propose that fire in arctic ecosystems may also be an important mechanism for amplifying arctic surface temperatures during the Pliocene, and so seek to understand its characteristics through quantification from the sediment record.

Although it is generally thought that atmospheric CO_2 concentrations of ~ 400 ppm provided the dominant global radiative forcing during the mid-Pliocene, CO_2 proxies over the Pliocene do not all agree (Fig. 1). Reconstructions of Pliocene CO_2 range between 190 and 440 ppm (Martinez-Boti et al., 2015; Seki et al., 2010). While CO_2 estimates from stomata and paleosols tend to be less precise, they are within the range of boron and alkenone derived estimates (Royer, 2006; Foster et al. 2017). Due to this variation in estimates from approximately the same time and variation in CO_2 over time, there is no clear value for CO_2 concentration in Earth's atmosphere that can be assigned to broad periods during the Pliocene. Dating uncertainties are an additional confounding factor complicating site to site

comparisons. Although modelled direct effects of this level of CO_2 variation may be small (Feng et al., 2017), reconstructing the CO_2 from the same deposits from which paleoclimate and paleoecological proxies are derived, may help reconcile previous estimates and contribute to constraining climate sensitivities during the Pliocene.

To advance our understanding of arctic amplification during past warm intervals in Earth's history such as the Pliocene by providing data to support boundary conditions and for verification in ESMs, this investigation targets an exceptionally well-preserved arctic sedimentary sequence to simultaneously reconstruct atmospheric CO_2, summer temperature, vegetation and fire from a single site.

2 Methods

2.1 Site description

To investigate the environment and climate of the Pliocene Arctic we focused on the Beaver pond (BP) fossil site, located at 78° 33′ N (Fig. 2) on Ellesmere Island. The stratigraphic section located at ~380 meters above sea level (MASL) today includes unconsolidated bedded sands and gravels, and rich organic layers including a fossil rich peat layer, up to 2.4 m thick, with sticks gnawed by an extinct beaver (*Dipoides spp.*). The assemblage of fossil plants and animals at BP has been studied extensively to gain insight into the past climate and ecology of the Canadian High Arctic (Ballantyne et al., 2006; Csank et al., 2011a; Csank et al., 2011b; Fletcher et al., 2017; Mitchell et al., 2016; Rybczynski et al., 2013; Tedford and Harington, 2003; Wang et al., 2017). Previous paleoenvironmental evidence suggests the main peat unit is a rich fen deposit with a neutral to alkaline pH, associated with open water (Mitchell et al., 2016), likely a lake edge fen or shallow lake fen, within a larch-dominated forest-tundra environment (Matthews and Fyles, 2000), not a low pH peat-bog. While the larch species identified at the site, *Larix groenlandia*, is extinct (Matthews and Fyles, 2000), many other plant remains are Pliocene examples of taxa that are extant (Fletcher et al., 2017).

The fen-peat unit examined in this study was sampled in 2006 and 2010. The main sequence examined across the methods used in this study includes material from Unit II, the entire span of Unit III, and material from Unit IV sampled from Section A as per Mitchell et al. (2016; Fig. S1; see Mitchell et al. 2016 Fig 5), with a total sampled profile of 1.65 m. Unit III has been estimated to represent ~20 000 years of deposition based on modern northern fen growth rates (Mitchell et al., 2016). The atmospheric CO_2 estimates from this locality were based on 22 sample layers from the 2006 field campaign, and the charcoal was based on 31, while the temperature estimates from specific bacterial membrane lipids were taken from 22 of the sample layers collected in 2006 and an additional 12 samples collected in 2010. The same samples from the 2006 season were analyzed for each of CO_2, mean summer temperature and char count where contents of the sample allowed. Pollen was tabulated from 10 samples from the 2006 sequence, located at different stratigraphic depths.

2.2 Geochronology

While direct dating of the peat was not possible, we were able to establish a burial age for fluvial sediments deposited approximately 4–5 m above and 30 m to the southwest of the peat. We used a method based on the ratio of isotopes

produced in quartz by secondary cosmic rays. The cosmogenic nuclide burial dating approach measures the ratio of cosmogenic ^{26}Al (t½ = 0.71 Ma) and ^{10}Be (t½ = 1.38 Ma) in quartz sand grains that were exposed on hillslopes and alluvium prior to final deposition at BP. Once the quartz grains are completely shielded from cosmic rays, the ratio of the pair will predictably decrease because ^{26}Al has double the radiodecay rate of ^{10}Be. In 2008, four of the medium to coarse grained quartz samples were collected from a vertical profile of planar crossbedded fluvial sands between 8.7 and 10.4 m below the overlying till surface. The samples were 5 cm thick, separated by an average of 62 cm, and should closely date the peat (the sandy braided stream beds represent on the order of ~10^4 years from the top of the peat to the highest sample). Quartz concentrates were extracted from the arkosic sediment using Frantz magnetic separation, heavy liquids, and differential leaching with HF in ultrasonic baths. When sample aliquots reached aluminum concentrations <100 ppm (ICP-OES) as a proxy of feldspar abundance, the quartz concentrate was subjected to a series of HF digestion and rinsing steps to ensure that more than 30% of the quartz had been dissolved to remove meteoric ^{10}Be. Approximately 200 mg of Be extracted from a Homestake Gold Mine beryl-based carrier was added to 150 g of each quartz concentrate (no Al carrier was needed for these samples). Such large quartz masses were digested because of the uncertainty in the abundance of the faster decaying isotope. Following repeated perchloric-acid dry-downs to remove unreacted HF, pH-controlled precipitation, column chemistry ion chromatography to extract the Be and Al ions, precipitation in ultrapure ammonia gas, and calcination at temperatures above 1000°C in a Bunsen flame for three minutes, oxides were mixed with equal amounts of niobium and silver by volume. These were packed into stainless steel targets for measurement at Lawrence Livermore National Laboratory's accelerator mass spectrometer (AMS). Uncertainty estimates for $^{26}Al/^{10}Be$ were calculated as 1σ by combining AMS precision with geochemistry errors in quadrature. For a complete detailed description of TCN methods see Rybczynski et al. (2013). The ages provided here are updated from Rybczynski et al. (2013) by using more recent production rate information and considering the potential for increasing exposure to deeply penetrating muons during the natural post-burial exhumation at BP.

2.3 Atmospheric CO_2 Reconstruction

In order to reconstruct atmospheric CO_2 concentrations during the Pliocene, we derived a method based on the different sensitivity of isotopic discrimination of plant groups to their environment (Farquhar et al., 1989; Fletcher et al., 2008; White et al., 1994). Specifically, we used measurements of stable carbon isotopic discrimination in C3 vegetation to approximate the carbon isotopic signature of the atmosphere, and measurements of carbon isotopic discrimination in bryophytes to estimate the partial pressure of atmospheric CO_2, which was then converted to atmospheric CO_2 concentration. According to theory (Farquhar et al., 1989), plants discriminate ~~($\Delta\ ^{13}C$)~~ against the heavier isotope in atmospheric CO_2, such that:

$$\Delta = a + (b - a)\frac{p_i}{p_a} \qquad (1)$$

where the fractionation~~s~~ of atmospheric CO_2 due to diffusion (a = ~ -4.4 ‰) and carboxylation by the enzyme rubisco (b = ~ -27 ‰) are constraints. Thus, ~~isotopic fractionation~~ in C3 plants ($\Delta\ ^{13}C_{C3}$) is largely a function of stomatal

control of partial pressure of intercellular CO_2 – (p_i) with respect to the partial pressure of atmospheric CO_2 (p_a). However, bryophytes lack stomata and thus a mechanism for actively regulating p_i, such that isotopic fractionation ($\Delta^{13}C_{bryo}$) varies mainly as a function of partial pressure ~~in~~ atmospheric CO_2 (i.e. p_a). While other environmental factors, such as humidity, temperature, light availability, and microclimate may also play important roles in isotopic discrimination in bryophytes (Fletcher et al., 2008; Ménot and Burns, 2001; Royles et al., 2014; Skrzypek et al., 2007; Waite and Sack, 2011; White et al., 1994), the first order control on discrimination is the partial pressure of atmospheric CO_2 (Fletcher et al., 2008; White et al., 1994). Because atmospheric CO_2 is relatively well mixed in the troposphere its mean annual concentration does not differ significantly by location. However, because total atmospheric pressure decreases with atmospheric height (h), the partial pressure of atmospheric CO_2 must also decrease according to the following exponential function:

$$p_{a(h)} = p_{a(i)} e^{-h/H} \quad (2)$$

such that the partial pressure of atmospheric CO_2 at any given height in the atmosphere ($p_{a(h)}$) can be calculated based on the initial atmospheric partial pressure of atmospheric CO_2 ($p_{a(i)}$) and a reference height (H = 7600 m), where atmospheric pressure goes to 0.37 Pa (Bonan, 2015). Therefore, assuming that carbon isotopic discrimination in bryophytes varies in response to the partial pressure of atmospheric CO_2 we can predict from basic physical principles an increase in $\Delta^{13}C_{bryo}$ in response to an increase in $p_{a(h)}$. Furthermore, if the assumptions of this empirical relationship are valid, then this empirical relationship can in theory be used to predict the partial pressure of atmospheric CO_2 based on carbon isotopic measurements of bryophytes.

To test this prediction, we compiled data from four studies investigating carbon isotopic variability of different bryophytes, primarily mosses, along elevational transects at different locations. Based on the elevations and locations of moss samples, the atmospheric partial pressure of atmospheric CO_2 was estimated from ERA-interim reanalysis data of total atmospheric pressure (Dee et al., 2011) in conjunction with globally averaged atmospheric CO_2 concentrations (Global View-CO_2, 2013) from the years moss samples were collected. For our analysis we only included measurements of carbon isotopic variability in non-vascular mosses and all isotopic values were normalized to cellulose based on the empirical relationship reported by Ménot and Burns (2001). Carbon isotopic discrimination values for all plant material was calculated as:

$$\Delta^{13}C = (\delta^{13}C_{atm} - \delta^{13}C_{plant})/(1 + \delta^{13}C_{plant}/1000) \quad (3)$$

where $\delta^{13}C_{plant}$ represents the C isotopic composition of plant cellulose and $\delta^{13}C_{atm}$ represents the mean annual carbon isotopic composition of atmospheric CO_2 of the year when samples were collected (Global View-CO_2, 2013), or in the case of sub-fossil mosses, when the samples were growing. The response $\Delta^{13}C$ to pCO_2 across elevational gradients in modern mosses was then used to calibrate the theoretical model BRYOCARB that has been developed to reconstruct past CO_2 levels based on measurements of ^{13}C in paleo bryophytes. Thus, our approach provides two independent estimates of Pliocene CO_2 concentrations – one empirically derived from our transfer function and the

other predicted from the BRYOCARB model calibrated to modern mosses and constrained by our paleoclimate reconstructions.

In order to derive estimates of atmospheric CO_2 concentrations during the Pliocene, isotopic composition of source CO_2 from the atmosphere (ie. $\delta^{13}C_{atm}$) was estimated during the Pliocene to solve for $\Delta\ ^{13}C$ of mosses (Eq.(3)). This was accomplished by simultaneous measurements of $\delta^{13}C$ in the C3 plant buckbean (*Menyanthes trifoliata* L.) that was identified as a subfossil specimen at the BP site and was also collected from four different sites in the Canadian Boreal Forest. Although it has been demonstrated that ~~$\Delta\ ^{13}C$~~ of C3 plant ~~material~~ is sensitive to many factors, including mean annual precipitation and altitude (Diefendorf et al. 2010), there is less variability within biomes, so modern buckbean was sampled from within the Canadian Boreal biome that we suspect is very similar to the BP site based upon paleovegetation (Ballantyne et al. 2010, Fletcher et al. 2017). Measurements of $\delta^{13}C$ on modern buckbean were used to constrain estimates of p_i / p_a using modern estimates of $\delta^{13}C_{atm}$ from when the buckbeans were collected. This constrained modern value of p_i / p_a was then applied to our sub-fossil buckbean samples to estimate $\delta^{13}C_{atm}$ during the Pliocene. All plant and moss material were rinsed and placed in a sonicating bath with deionized water to remove any paleosoil from samples. The diagnostic material for mosses was leafy material, whereas buck bean was identified based on seeds. Therefore, to ensure that our isotopic measurements were made on similar compounds, cellulose was extracted from samples according to Leavitt and Danzer (1993). All carbon isotopic measurements were performed at University of Arizona's environmental isotope laboratory.

2.4 Paleotemperature Reconstruction

Paleotemperature estimates were determined based on the distribution of fossilized, sedimentary membrane lipids known as branched glycerol dialkyl glycerol tetraethers (brGDGTs) that are well preserved in peat bogs, soils, and lakes (Powers et al., 2004; Weijers et al., 2007c). These unique lipids are thought to be synthesized by a wide array of Acidobacteria within the soil (Sinninghe Damsté et al., 2011; Sinninghe Damsté et al., 2014) and presumably other bacteria (Sinninghe Damsté et al., 2018) in soils and peat bogs but also in aquatic systems. Previously, it has been established that the degree of methyl branching (expressed in the methylation index of branched tetraethers; MBT) is correlated with mean annual air temperature (MAT), and the relative amount of cyclopentane moieties (expressed in the cyclization index of branched tetraethers; CBT) has been shown to correlate with both soil pH and mean annual air temperature (Weijers et al., 2007b). Because of the relationship of the distribution of these fossilized membrane lipids with these environmental parameters, it has been used for paleoclimate applications in different environments including coastal marine sediments (Bendle et al., 2010; Weijers et al., 2007a), peats (Ballantyne et al., 2010; Naafs et al., 2017), paleosols (Peterse et al., 2011; Zech et al., 2012), and lacustrine sediments (Loomis et al., 2012; Niemann et al., 2012; Pearson et al., 2011; Zink et al., 2010).

Improved separation methods (Hopmans et al., 2016) have recently led to the separation and quantification of the 5- and 6-methyl brGDGT isomers that used to be treated as one since the 6-methyl isomers were co-eluting with the 5-methyl isomers (De Jonge et al., 2013). This has led to the definition of new indices and improved MAT calibrations based on the global soil (De Jonge et al., 2014), peat (Naafs et al., 2017), and African lake (Russell et al., 2018) datasets.

Sediment samples were freeze-dried and then ground and homogenized with a mortar and pestle. Next, using the Dionex™ accelerated solvent extraction (ASE), 0.5–1.0 g of sediment was extracted with the solvent mixture of dichloromethane (DCM):methanol (9:1, v/v) at a temperature of 100°C and a pressure of 1500 psi (5 min each) with 60% flush and purge 60 s. ~~The~~ Caliper Turbovap®LV was utilized to concentrate the collected extract, which was then transferred using DCM and dried over anhydrous Na_2SO_4 before being concentrated again under a gentle stream of N_2 gas. To quantify the amount of GDGTs, 1 µg of an internal standard (C46 GDGT; Huguet et al., 2006) was added to the total lipid extract. Then, the total lipid extract was separated into three fractions using hexane:DCM (9:1, v:v) for the apolar fraction, hexane:DCM (1:1, v:v) for the ketone fraction and DCM:MeOH (1:1, v:v) for the polar fraction, using a column composed of Al_2O_3, which was activated for 2 h at 150°C. The polar fraction, which contained the GDGTs, was dried under a steady stream of N_2 gas and weighed before being ~~then~~ re-dissolved in hexane:isopropoanol (99:1, v:v) at a concentration of 10 mg ml^{-1} and subsequently passed through a 0.45 µm PTFE filter. Finally, the polar fractions were analyzed for GDGTs by ultra-high performance liquid chromatography – atmospheric pressure positive ion chemical ionization – mass spectrometry (UHPLC-APCI-MS) using the method described by Hopmans et al., (2016). The polar fractions of some samples were re-run on the UHPLC-APCI-MS multiple times and the average fractional abundances of the brGDGTs was determined.

For the calculation of brGDGT-based proxies, the brGDGTs are specified by the Roman numerals as indicated in Fig. S2. The 6-methyl brGDGTs are distinguished from the 5-methyl brGDGTs by a prime. The novel indices, including MBT'_{5Me} based on just the 5-methyl brGDGTs and the CBT′ that was used to calculate the pH (De Jonge et al., 2014):

$$MBT'_{5Me} = ([Ia] + [Ib] + [Ic]) / ([Ia] + [Ib] + [Ic] + [IIa] + [IIb] + [IIc] + [IIIa] + [IIIb] + [IIIc]) \quad (4)$$

$$CBT' = {}^{-10}\log[([Ic] + [IIa'] + [IIb'] + [IIc'] + [IIIa'] + [IIIb'] + [IIIc'])/([Ia] + [IIa] + [IIIa])] \quad (5)$$

The square brackets denote the fractional abundance of the brGDGT within the bracket relative to the total brGDGTs. Mean summer air temperature (MST) was determined using the distributions of aquatically produced brGDGTs in the lake calibration developed by Pearson et al. (2011). When this calibration is used the fractional abundances of IIa and IIa′ must be summed because these two isomers co-eluted under the chromatographic conditions used by Pearson et al. (2011):

$$MST\ (°C) = 20.9 + 98.1 \times [Ib] - 12 \times ([IIa] + [IIa']) - 20.5 \times [IIIa] \quad (6)$$

MAT and surface water pH were also calculated using a novel calibration created using sediments from East African lakes analysed with the novel chromatography method and based upon MBT'_{5Me} (Russell et al., 2018).

$$MAT = -1.2141 + 32.4223 * MBT'_{5Me} \quad (7)$$

$$\text{Surface water pH} = 8.95 + 2.65 * CBT' \quad (8)$$

2.5 Vegetation and Fire Reconstruction

For charcoal, a total of thirty 2 cm^3 samples were taken at 5 cm intervals from depths from 300 and 301.45 MASL at the BP site, with an additional 2cm^{-3} sample collected at 301.65 MASL. All samples were deflocculated using sodium hexametaphosphate and passed through 500, 250 and 125 µm nested mesh sieves. The residual sample caught on each sieve was then collected in a gridded petri dish and examined using a stereomicroscope at 20-40X magnification to obtain charcoal concentration (fragments cm^{-3}). Charcoal area (mm^2 cm^{-3}) was measured for each sample using specialized imaging software from Scion Corporation. For a detailed description of methods see Brown and Power (2013).

Vegetation was reconstructed using pollen and spores (herein pollen) at selected elevations chosen to capture upper and lower sections of the elevation profile, and that corresponded with changes in charcoal. The sample depths selected for pollen analyses were 300.3–300.4 MASL, 301.10–301.25 MASL, and 301.35–301.45 MASL. Samples were processed using standard approaches (Moore et al., 1991), whereby 1cm^3 sediment subsamples were treated with 5% KOH to remove humic acids and break up the samples. Carbonates were dissolved using 10% HCl, whereas silicates and organics were removed by HF and acetolysis treatment, respectively. Pollen slides were made by homogenizing 35 µl of residue, measured using a single-channel pipette, with 15 µl of melted glycerin jelly. Slides were counted using a Leica DM4000 B LED compound microscope at 400–630x magnification. A reference collection and published keys (McAndrews et al., 1973; Moore et al., 1991) aided identification.

In addition to tabulating pollen and charcoal, a list of plant taxa derived from Beaver Pond was previously compiled in Fletcher et al. (2017). Extant species from this list were selected and their modern occurrences extracted from the Global Biodiversity Information Facility (GBIF.org, 2017). Observation data was grouped by 5° latitude 5° longitude grids cells, and the shared species count calculated using R (R Core Team, 2016). Modern fire frequency was mapped using the MODIS 6 Active Fire Product. The fire pixel detection count per day, within the same 5° latitude 5° longitude grids cells was counted over the ten years 2006–2015, and standardized by area of the cell. The modern climate maps were generated using data from WorldClim 1.4 (Hijmans et al., 2005). The values for the bioclimatic variables mean temperature of the warmest quarter (equivalent to mean summer air temperature; MST) and precipitation of the warmest quarter (summer precipitation) were also averaged by grid cell. The shared species count, climate values, and fire day detections were mapped to the northern polar stereographic projection in ArcMap 10.1.

3 Results

3.1 Geochronology

The burial dating results with $^{26}Al/^{10}Be$ in quartz sand at 10 m below modern depth provides four individual ages. From shallowest to deepest, the burial ages are 3.6 +1.5/-0.5 Ma, 3.9 +3.7/-0.5 Ma, 4.1 +5.8/-0.4 Ma, and 4.0 +1.5/-0.4 Ma (Table S2), with an unweighted mean age of 3.9 Ma. The convoluted probability distribution function yields a maximum probability age of 4.5 Ma. Unfortunately, the positive tails of the probability distribution functions of two of the samples exceeds the radiodecay saturation limit of the burial age. Therefore, their probability distributions do not reflect the actual age probabilities and uncertainty. Given the positive tail in the probability distribution functions,

and the inability to convolve all samples, we recommend using the unweighted mean age, 3.9 Ma, with an uncertainty of +1.5/-0.5 Ma as indicated by the two samples with unsaturated limits. Despite the apparent upward younging of the individual burial ages, the 1σ-uncertainties overlap rendering the samples indistinguishable.

3.2 Atmospheric CO_2 Reconstruction

As expected, carbon isotopic discrimination in mosses shows a positive relationship with partial pressure of atmospheric CO_2 both in empirical observations and theoretical predictions (Fig. 3). However, a much greater change in $\Delta^{13}C_{moss}$ is observed in response to p_a than is predicted from the optimized BRYOCARB simulations. The empirical fit to the observed change in $\Delta^{13}C_{moss}$ in response to p_a is slightly better (RMSE = 1.8 ‰) than the theoretical prediction from the BRYOCARB model (RMSE = 2.1 ‰), but the slopes are quite different, with our empirical slope (0.56 ‰/p_a) an order of magnitude greater than the linear approximation of the BRYOCARB slope (0.07 ‰/p_a), suggesting that other non-linear processes and not just p_a may be affecting $\delta^{13}C_{moss}$ variability with elevation.

While there does appear to be a global relationship between p_a and $\Delta^{13}C$ of mosses, there are notable differences among sites. Moss $\Delta^{13}C$ values tended to be generally lower in the Swiss Alps (mean = 17.4 ‰) and higher in Hawaii (mean = 20.6 ‰) and the slope of the relationship between p_a and $\Delta^{13}C$ appears to vary across sites with the Andes having the smallest slope and Poland having a much greater slope. We used the BRYOCARB model to test the sensitivity of $\Delta^{13}C$ to other variables that change as a function of elevation (e.g. temperature and pO_2). According to our BRYOCARB simulations, with all other variables held constant decreased temperature with increased elevation should slow metabolic rates resulting in an increase in $\Delta^{13}C$ (Fig. S3), which directly contradicts observations (Fig. 3). Furthermore, the range of mean summer temperature estimates from the Pliocene BP site could only explain ~0.2 ‰ isotopic response in our moss samples. Similarly we evaluated the effect of just changing pO_2 in our BRYOCARB simulations and found a decrease in $\Delta^{13}C$ with increasing pO_2 that is opposite to the $\Delta^{13}C$ response of mosses to partial pressure across all elevational transects. We also evaluated model performance using a global standard atmospheric sea level pressure of 101.325 kPa, or site-specific atmospheric pressure estimates from ERA-interim reanalysis data. We found that the model using site specific atmospheric pressure estimates performed better at predicting $\Delta^{13}C_{moss}$ (RMSE = 1.096 ‰) than the model using global standard atmospheric sea level pressure (RMSE = 1.216 ‰). Therefore, it appears that partial pressure of atmospheric CO_2 is the primary physical mechanism explaining the global relationship between $\Delta^{13}C$ of mosses and elevation and that other factors, such as water availability that may be mediated by different lapse rates (Ménot and Burns, 2001; Royles et al., 2014; Skrzypek et al., 2007; Waite and Sack, 2011), may explain variability among sites. Thus, the optimal model characterizing the observed modern relationship between $\Delta^{13}C_{moss}$ and the p_a was:

$$^{13}C\ \Delta^{13}C_{\mathrm{moss}} = 0.56 \times pCO_2 + 1.55 \qquad (9)$$

Based on our analysis of cellulose extracted from four different *Menyanthes* L. (i.e. buckbean) plants growing at four different locations in the modern boreal forest, we found $\Delta^{13}C$ of buckbean to be fairly constant 16 ± 0.4 ‰, yielding an estimate of p_i / p_a in modern buckbean of 0.51. Applying this modern of p_i / p_a to our $\delta^{13}C$ measurements

from sub-fossil buckbean we obtained estimates of $\delta^{13}C_{atm}$ during the Pliocene of -6.23 ± 0.9 ‰. Using our empirical transfer function (Eq. 9) in combination with these estimates of $\delta^{13}C_{atm}$, we were able to approximate atmospheric CO_2 concentrations over the Pliocene interval captured at the BP site (Fig. 4). We estimated a mean atmospheric CO_2 concentration over this interval of 410 ± 50 ppm (mean ± transfer error and instrument error) with considerable variability between a minimum atmospheric CO_2 concentration of 296 ppm and a maximum atmospheric CO_2 concentration of 480 ppm. Predicted values of Pliocene CO_2 from the BRYOCARB model were slightly higher at 510 ppm, but the single standard deviation across all estimates was extremely high (967 ppm), suggesting that the BRYOCARB simulations are not significantly different from our empirical model estimates; however, the BRYOCARB model is too sensitive to our range of $\Delta^{13}C_{moss}$ estimates and thus not very precise.

3.3 Paleotemperature Estimates

3.3.1 Provenance of branched GDGTs

Previously, brGDGT derived MAT estimates (-0.6 ± 5.0 °C) from BP sediments were developed using the older chromatography methods that did not separate the 5- and 6- methyl brGDGTs, and a soil calibration (Ballantyne et al., 2010). In marine and lacustrine sediments, bacterial brGDGTs were thought to originate predominantly from continental soil erosion arriving in the sediments through terrestrial runoff, however, a number of more recent studies have indicated aquatically produced brGDGTs could be affecting the distribution of the sedimentary brGDGTs and thus the temperature estimates based upon them (Warden et al., 2016; Zell et al., 2013; Zhu et al., 2011). Since the discovery that sedimentary brGDGTs can have varying sources, different calibrations have been developed depending on the origin of the brGDGTs, i.e. soil calibration (De Jonge et al., 2014), peat calibration (Naafs et al., 2017) and aquatic calibrations (i.e. Foster et al., 2016; Pearson et al., 2011; Russell et al., 2018). Therefore, several studies have recommended that the potential sources of the sedimentary brGDGTs should be investigated before attempting to use brGDGTs for paleoclimate applications (De Jonge et al., 2015; Warden et al., 2016; Yang et al., 2013; Zell et al., 2013). In this study, we examine the distribution of brGDGTs in an attempt to determine their origin and consequently the most appropriate calibration to utilize in order to reconstruct temperatures from the BP sediments.

Branched GDGTs IIIa and IIIa′ on average had the highest fractional abundance of the brGDGTs detected in the BP sediments (see Fig. S2 for structures; Table S4). A previous study established that when plotted in a ternary diagram the fractional abundances of the tetra-, penta- and hexamethylated brGDGTs, soils lie within a distinct area (Sinninghe Damsté, 2016). To assess whether the brGDGTs in the BP deposit were predominantly derived from soils, we compared the fractional abundances of the tetra-, penta- and hexamethylated brGDGTs in the BP sediments to those from modern datasets in a ternary diagram (Fig. 5). Since the contribution of brGDGTs from either peat or aquatic production could affect the use of brGDGTs for paleoclimate application, in addition to comparing the samples to the global soil dataset (De Jonge et al., 2014), peat and lacustrine sediment samples were added into the ternary plot to help elucidate the provenance of brGDGTs in the BP sediments. According to Sinninghe Damsté (2016), it is imperative to only compare samples in a ternary diagram like this where all of the datasets were analyzed with the novel methods that separate the 5- and 6-methyl brGDGTs since the improved separation can result in an increased abundance of hexamethylated brGDGTs. Recently, samples from East African lake sediments were analyzed using

these new methods (Russell et al., 2018) and so these samples were included in the ternary plot for comparison (Fig. 5). Although the lakes from the East African dataset are all from a tropical area, they vary widely in altitude and, thus, in MAT. We separated them into three categories by MAT (lakes >20°C, lakes between 10-20°C and lakes<10°C). By comparing all the samples in the ternary plot, it was evident that the BP samples plotted closest to the lacustrine sediment samples from regions in East Africa with a MAT <10°C, suggesting that the provenance of the majority of the brGDGTs from the BP sediments was not soil or peat but lacustrine aquatic production.

The average estimated surface water pH for the BP sediments (8.6±0.2) calculated using eq. (8), is within the 6 –9 range typical of lakes and rivers (Mattson, 1999). This value is near the upper limit of rich fens characterized by the presence of *S. scorpioides* (Kooijman and Westhoff, 1995; Kooijman and Paulissen, 2006) and is higher than what would be expected for peat-bog sediments that are acidic (pH 3–6; Clymo, 1964) and which constitute most of the peats studied by Naafs et al. (2017). A predominant origin from lake aquatic production is in keeping with previous interpretation of the paleoenvironment of the BP site, which was at least at times covered by water as evidenced by fresh water diatoms, fish remains and gnawed beaver sticks in the sediment (Mitchell et al., 2016).

3.3.2 Aquatic Temperature Transfer Function

Since there is evidence that the majority of the brGDGTs in the BP sediments are aquatically produced, an aquatic transfer function was used for reconstructing temperature. When we apply the African lake calibration (Eq. 7), the resulting estimated MAT for BP is 7.1 ± 1.0 °C. This value is high compared to other previously published estimates from varying proxies, which have estimated MAT in this region to be in the range of -5.5 to 0.8°C, (Ballantyne et al., 2010; Ballantyne et al., 2006; Csank et al., 2011a; Csank et al., 2011b; Fletcher et al., 2017). A concern when applying this calibration is that it is based on lakes from an equatorial region that does not experience substantial seasonality, whereas, the Pliocene Arctic BP site did experience substantial seasonality (Fletcher et al., 2017). Biological production (including brGDGT production) in BP was likely skewed towards summer and, therefore, summer temperature has a larger influence on the reconstructed MAT. Unfortunately, no global lake calibration set using individually quantified 5- and 6-methyl brGDGTs is yet available. Therefore, to calculate mean summer air temperatures (MST, Eq. 6) we applied the aquatic transfer function developed by Pearson et al. (2011) by combining the individual fractional abundances of the 5- and 6-methyl brGDGTs. The Pearson et al. (2011) calibration was based on a global suite of lake sediments including samples from the Arctic, thus covering a greater range of seasonal variability. The resulting average estimated mean summer temperature was 15.4 ± 0.8 °C, with temperatures ranging between 14.1 and 17.4 °C (Fig. 4). This is in good agreement with recent estimates based on Climate Reconstruction Analysis using Coexistence Likelihood Estimation (CRACLE; Fletcher et al., 2017) that concluded that MSTs at BP during the Pliocene were approximately 13 to 15°C.

3.4 Vegetation and Fire Reconstruction

All sediment samples from BP contained charcoal (Fig. 4), indicating the consistent prevalence of biomass burning in the High Arctic during this time period. However, counts were variable throughout the section, with the middle and lower sections (18 fragments cm^{-3}) containing less charcoal compared to the upper section upper section (710

fragments cm^{-3}). Overall, samples from BP contained on average 100.0 ± 165 fragments cm^{-3} (mean ± 1 σ), with charcoal area averaging 12.3 ± 20.2 mm^2 cm^{-3}. The variability of charcoal within any given sample was relatively low with a 1 σ among charcoal area of approximately 2 mm^2 cm^{-3}.

The three parts of the section analysed for pollen (300.3–300.4 MASL, 301.15–301.25 MASL, and 301.35–301.45 MASL) reveal variations in vegetation (Figs. 4 and 6). Near the bottom of the section (300.3-300.4 MASL), *Larix* (26%) and *Betula* (17%) were the dominant trees. *Alnus* (6%) and *Salix* (6%) together with ericaceous pollen (4%) were relatively high. In contrast, low numbers of *Picea* (3%), *Pinus* (3%) and fern spores were recorded. Additional wetland taxa like *Myrica* (5%) and Cyperaceae (6%) were also noted. Overall, the non-arboreal (23%) signal was well developed. Crumpled and/or ruptured inaperturate grains with surface sculpturing that varied from scabrate to verricate were noted in the assemblage (12%), but could not be definitely identified. It is possible that these grains represent *Populus*, Cupressaceae or additional Cyperaceae pollen. Between 301.10-301.25 MASL, *Larix* (38%) and *Betula* (21%) increased in abundance, followed by ferns (7%). Cyperaceae remained at similar levels (6%) whereas *Picea* and *Pinus* decreased to 2% and 1%, respectively. Unidentified inaperturate types collectively averaged 14%. *Larix* pollen (23%) remained abundant near the top of the section (301.35-301.45 MASL), whereas *Betula* (2%) decreased. *Picea* (16%) *Pinus* (6%) and ferns (23%) increased in abundance. Of the ferns, trilete spores and cf. *Botrychium* were most abundant, followed by cf. *Dryopteris*. Inaperturate unknowns (10%) were also observed. Other notables included Ericaceae (2%) and Cyperaceae (2%). While rare, Onagraceae grains were also observed (Fig. 6).

According to GBIF-based mapping exercise, the paleofloral assemblage at BP most closely resembles modern day vegetation found in northern North America, particularly on the eastern margin (e.g. New Hampshire, New Brunswick and Nova Scotia) and the western margin (Alaska, Washington, British Columbia, and Alberta; Fig. 7a), and central Fennoscandia. Of these areas, the western coast of northern North America and eastern coast of southern Sweden has the most similarity to the reconstructed BP climate in terms of MST (Fig. 7b) and summer precipitation (Fig. 7c).

While high counts of active fire days are common in the western part of the North American boreal forest, it is not as common in the eastern part of the North American boreal forest (Fig. 7d), likely due to the differences in the precipitation regime. There was also low fire counts in Fennoscandia likely due to historical severe fire suppression (Brown and Giesecke, 2014; Niklasson and Granström, 2004). Therefore, based on our reconstruction of the climate and ecology of the BP site, our results suggest that BP most closely resembled a boreal-type forest ecosystem shaped by fire, similar to those of Washington, British Columbia, Northwest Territories, Yukon and Alaska (but see Sect. 4.3).

4 DISCUSSION

4.1 Geochronology

The plant and animal fossil assemblages observed at BP suggest a depositional age between 3 and 5 Ma (Matthews Jr and Ovenden, 1990; Tedford and Harington, 2003). This biostratigraphic age was corroborated with an amino-acid racemization age (>2.4 ± 0.5 Ma) and Sr-correlation age (2.8–5.1 Ma) on shells (Brigham-Grette and Carter, 1992) in biostratigraphically correlated sediments on Meighen Island, situated 375 km to the west-north-west. The previously

calculated burial age of 3.4 Ma for the BP site is a minimum age because no post-depositional production of ^{26}Al or ^{10}Be by muons was assumed. If the samples are considered to have been buried at only the current depth (ca. 10 m, see supplemental data) then the ages plot to the left and outside of the burial field, indicating that the burial depth was significantly deeper for most of the post-depositional history. The revised cosmogenic nuclide burial age is 3.9 +1.5/-0.5 Ma. It is the best interpretation of burial age data based on improved production rate systematics (e.g. Lifton et al., 2014), and more reasonable estimates of erosion rate and ice cover since the mid-Pliocene (see Fig. S4; Table S5). As the stratigraphic position of the cosmogenic samples is very close to the BP peat layers, we interpret the age to represent the approximate time that the peat was deposited.

4.2 Pliocene atmospheric CO_2 levels

We have derived a transfer function that allows us to predict the partial pressure of atmospheric CO_2 in Earths' past based on carbon isotopic measurements in byrophytes. However, many of the studies included in our transfer function identify other mechanisms that may also influence carbon isotopic discrimination in bryophytes. Because these other mechanisms may violate the assumptions of applying this transfer function to the past or contribute error to our reconstructions of atmospheric CO_2 concentrations during the Pliocene, we discuss these mechanisms below.

It has been suggested that in the absence of stomatal regulation, that surface water may control the gradient in partial pressure (i.e. p_i / p_a) in bryophytes (White et al., 1994), due to the greater resistance to diffusion of CO_2 in water than in the atmosphere. For instance, Ménot and Burns (2001) found that most mosses growing along an elevational transect in Switzerland experienced discrimination with elevation in response to decreased partial pressure, except one species *Sphagnum cuspidatum* Ehrh. ex Hoffm., which grows almost exclusively in wet hollows. In a study of Hawaiian bryophytes Waite and Sack (2011) found consistent slopes of less isotopic discrimination with elevation in all species, however, species growing on young substrate showed significantly less isotopic discrimination. The most likely explanation is that lack of canopy cover on the older substrates lead to greater photosynthetic rates, which lead to reduced p_i. Lastly, decreased discrimination of mosses growing along an elevational transect in Poland (Skrzypek et al., 2007), was found to be highly correlated with temperature. Although temperature is the primary factor driving most metabolic reactions, it does not provide a physical mechanism explaining the relationship between elevation and isotopic discrimination in mosses. Skrzypek et al. (2007) found slightly different relationships between elevation and carbon isotopic discrimination in mosses growing on the windward versus leeward side of their elevational transects suggesting that changes in lapse rate may also play a factor. Collectively, these studies suggest that microclimatic factors may explain differences in isotopic discrimination of mosses within and among different sites possibly contributing to different intercepts for sites reported in Fig. 3, and that dry vs. moist lapse rates may also play a role in regulating the different slopes among sites. In fact, the greatest elevational range reported among sites was for the elevational transect in the Andes (320 to 3100 m), but this site did not experience the widest range in $\Delta^{13}C_{moss}$. This tropical transect had a very moist lapse rate resulting in the least change in atmospheric temperature and humidity with elevation. Nonetheless, by projecting these data as a function of partial pressure we provide a physical mechanism to explain variations in moss carbon isotopic values globally and we help reconcile the previously reported empirical relationships, such as elevation, temperature, and over-story, all of which tend to be covariates of decreasing partial

pressure with elevation. While differences in microclimate and lapse rate are clearly important factors in regulating $\Delta^{13}C_{moss}$, these factors contribute to the global error in our model for predicting p_a and ultimately to uncertainties in our estimates of atmospheric CO_2 concentrations during the Pliocene.

Our reconstructions of CO_2 concentration for this mid-Pliocene interval are within the range of previously reported CO_2 estimates, tending to agree with alkenone estimates from Pagani et al. (2010). This suggests that CO_2 concentrations during this warm Pliocene interval were above 400 ppm. In fact, our mean Pliocene value (410 ± 50 ppm) is not statistically different from the alkenone based estimates (357 ± 47 ppm) previously reported by Pagani et al. (2010) and our theoretical predictions based on BRYOCARB calibrated to modern $\Delta^{13}C_{moss}$ values indicate CO_2 concentrations of approximately 510 ppm, albeit ~~highly variable~~ due to the sensitivity of the model simulations. Generally, our estimates showed sustained atmospheric CO_2 estimates of slightly higher than 400 ppm with only two anomalously low values (Fig. 4). These estimates could represent an actual reduction in atmospheric CO_2, or they might be artefacts of sampling or analysis. It should be noted that poor preservation and a possible shift in dominant moss species to *Drepanocladius spp*. was evident in samples corresponding to these two anomalously low CO_2 estimates. While one of these samples contained only 0.17 mg/C and a $\delta^{13}C$ value of -20.9 ‰, the other contained 0.88 mg/C and a $\delta^{13}C$ value of -25.0 ‰. Thus, it is conceivable that the sample corresponding to the atmospheric CO_2 estimate of 355 ppm, might be approaching our minimum detection limit and should be verified in subsequent studies.

It should also be noted that changes in growth rate due to phosphorus availability and biases in shell size are known to contribute uncertainty to alkenone-derived CO_2 concentration estimates (Seki et al., 2010). Similar assumptions may affect boron-derived estimates of CO_2 concentrations. For instance, a recent update on the global boron cycle estimates the mean residence time of boron to be ~ 1.5 Ma and suggests that boron isotopes may not be sensitive to ocean pH on timescales less than 1 Ma (Schlesinger and Vengosh, 2016). This may help explain the apparent lack of variability in boron isotope based CO_2 estimates during the Pliocene (Hönisch et al., 2009; Tripati et al., 2009); however, boron isotopes do seem to reproduce the CO_2 variability measured in ice cores over the Pleistocene (Hönisch et al., 2009). Overall, our estimates using two independent approaches suggest that Pliocene CO_2 concentrations during this interval ranged between 400 and 500 ppm are consistent with recent estimates derived from both alkenones and from boron isotopes (Martinez-Boti et al., 2015; Seki et al., 2010).

There are numerous assumptions based on known uncertainties in our CO_2 reconstruction approach. First of all, our empirically based approach requires some estimate of the isotopic ratio of atmospheric CO_2 during this time, which we derive from C3 vegetation (Fletcher et al., 2008; White et al., 1994). Here we estimate the isotopic composition of the atmosphere over the Pliocene to be $\delta^{13}C = -6.23 \pm 0.9$ ‰, which is within the range of values recorded over glacial-interglacial intervals in ice cores $\delta^{13}C = -6.2$ to -7.0 ‰ (Bauska et al., 2016) and consistent with estimates derived from carbon isotope measurements of foraminifera (Ravelo et al., 2004). If we assume that the isotopic composition of atmospheric CO_2 was -8.2 ‰ during the Pliocene and similar to today due to greater transfer of lighter carbon from the terrestrial reservoir to the atmospheric reservoir, that would result in reduced $\Delta^{13}C_{moss}$ and decreases in our mean estimate of atmospheric CO_2 to approximately 390 ppm. This adjustment to our original estimate of $\delta^{13}C$ of atmospheric CO_2 would bring our atmospheric CO_2 estimate more in line with previous reconstructions, but is still within the range of error of our original estimate.

Another critical assumption of our approach is that the total pressure of the atmosphere has not changed at the BP site since the Pliocene either through increased partial pressure of constituent gases or more likely through changes in elevation due to dynamic isostacy. The current elevation of the site is approximately 380 MASL with a summertime total atmospheric pressure of approximate 88.5 kPa. If we assume that the site was at 0 m during the Pliocene that would increase the total summertime atmospheric pressure to 93.9 kPa and would decrease our Pliocene CO_2 estimates to about 390 ppm. However, estimates of dynamic eustacy since the Pliocene from paleoshorelines at lower latitudes are between 5 and 20 m (Rovere et al., 2014), suggesting that our assumptions regarding elevation at the site probably have a negligible impact on our estimates of Pliocene atmospheric CO_2 concentrations, especially given the uncertainty of the proxy approach. Therefore, the assumptions to our approach in estimating past CO_2 may be leading to estimates that are biased slightly high relative to previous estimates. When these assumptions are considered, our estimates still suggest atmospheric CO_2 concentrations around 400 ppm or above during this Pliocene warm interval.

4.3 Fire, vegetation, climate

Wildfire is a key driver of ecological processes in modern boreal forests (Flannigan et al., 2009; Ryan, 2002), and although historically rare, is becoming more frequent in the tundra in recent years (Mack et al., 2011). The modern increase in fire frequency is likely as a consequence of atmospheric CO_2 driven climate warming and feedbacks such as reduced sea ice extent (Hu et al., 2010), because the probability of fire is highest where temperature and moisture are conducive to growth and drying of fuels followed by conditions that favor ignition (Whitman et al., 2015). Young et al. (2017) confirmed the importance of summer warmth and moisture availability patterns in predicting fire across Alaska, highlighting a July temperature of ~13.5 °C as a key threshold for fire across Alaska.

The abundance of charcoal at BP demonstrates that climatic conditions were conducive for ignition and that sufficient biomass available for combustion existed across the landscape. brGDGTs-derived temperature estimates suggest mean summer temperatures at BP exceeded the ~13.5 °C threshold (Young et al., 2017) that drastically increases the chance of wildfire. An increase in atmospheric convection has been simulated in response to diminished sea-ice during warmer intervals (Abbot and Tziperman, 2008), but this study did not confirm if this increase in atmospheric convection was sufficient to cause lightning ignitions. An alternative ignition source for combustion of biomass on Ellesmere Island during the Pliocene is coal seam fires, which have been documented to be burning at this time (Estrada et al., 2009). However, given the interaction of summer warmth and ignition by lightning within the same climate range as posited for BP, we consider lightning the most likely source of ignition for Pliocene fires in the High Arctic.

Fire return intervals cannot be calculated from the BP charcoal counts due to the absence of a satisfactory age-depth model and discontinuous sampling. As strong interactions are observed between fire regime and ecosystem assemblage in the boreal forest (Brown and Giesecke, 2014; Kasischke and Turetsky, 2006), and in response to climate, comparison with modern fire regimes for areas with shared species compositions and climates may inform a potential range of mean fire return interval (MFRI).

Matthews and Fyles (2000) indicated that the Pliocene BP environment was characterized by an open larch dominated forest-tundra environment, sharing most species in common with those now found in three regions,

including central Alaska to Washington in western North America, the region centered around the Canadian/US border in eastern North America, as well as Fennoscandia in Europe. The modern area with the most species in common with BP is central northern Alaska (Fig. 7A). The area over which shared species were calculated is largely tundra, but includes the ecotone between tundra and boreal forest. Other zones that share many species with BP are continuous with Alaska down the western coast of North America to the region around the border of Canada and the United States, the eastern coast of North America in the region around the border of Canada and the United States (~50°N), and central Fennoscandia. Of these zones, the MST of Alaskan tundra sites (6–9°C) are less similar to BP (15.4°C) than ~50°N on both western and eastern coastal North American sites and central Fennoscandia (12–18°C, Fig. 7B). The eastern coast of North America has higher rainfall during the summer (>270 mm), than the west coast and Alaska (Fig. 7C), which correlates to the timing of western fires. The low summer precipitation for much of the west (<200 mm), is consistent with previously published summer precipitation estimates for BP (~190 mm). As a result, the fire regime of the west coast ~50°N may be a better analogue for BP than the east coast of North America. In central Fennoscandia there is also a west vs. east coastal variation in summer precipitation with the western, Nordic part of the region experiencing higher summer precipitation (252– >288 mm), than the more similar eastern, Swedish part of the region (~198 mm).

Comparison to modern fire detection data (Fig. 7D) suggests that the two regions most climatically similar to BP, ~50°N western North America and central Sweden, have radically different fire regimes. This is likely caused by historical fire suppression in Sweden that limits utility of very modern data for comparison in this study (Brown and Giesecke, 2014; Niklasson and Granström, 2004). To understand the fire regimes as shaped by climate and species composition rather than human impacts, we considered both the modern and recent Holocene reconstructions for these regions (Table 1). This shows that, a) within any region variation arises from the complex spatial patterning of fire across landscapes, and b) that the regions most similar to BP (~50°N western North American and eastern Fennoscandian reconstructions for the recent Holocene) have shorter fire return intervals than the cooler Alaskan tundra or wetter summer ~50°N eastern North American coast.

While the shared species for Siberia appears low, the number of observations in the modern biodiversity database used is likewise low – perhaps causatively so. Given the similar climate to BP on the Central Siberian Plateau and some key aspects of the floras in Siberia such as the dominance of larch, we considered the fire regime of the larch forests of Siberia. Kharuk et al. (2016; 2011) studied MFRIs across Siberia, from 64°N to 71°N, the northern limit of larch stands. They found an average MFRI across that range of 110 years, with MFRI increasing from 80 years in the southern latitudes to ~300 in the north (Table 1). Based on similarity of the climate variables, the more southerly MFRIs (~80 years) may be a better analogue. Key differences between boreal fires in the North America compared to Russia are a higher fire frequency with more burned area in Russia, but a much lower crown fire and a difference in timing of disturbance, with spring fires prevailing in Russia compared to mid-summer fires in western Canada (de Groot et al., 2013; Rogers et al., 2015).

The pollen-based vegetation reconstruction derived in this study indicates that open *Larix-Betula* parkland persisted in the basal (300.3-300.4 MASL) parts of the sequence. Groundcover was additionally dominated by shrub birch, ericaceous heath and ferns. While the regional climate may have been somewhat dry, the record suggests that, locally,

a moist fen environment dominated by Cyperaceae, existed near the sampling location. Shrubs including *Alnus* and *Salix* likely occupied the wetland margins.

The corresponding relatively low concentration of charcoal may reflect lower severity fires or higher sedimentation rates. We consider the former more likely due to the depositional environment of Unit III from Mitchell et al. 2016, a lake edge fen peat in a beaver pond or small lake, without evidence of high sediment influx overwhelming peat production. If the former, it is posited that a surface fire regime, somewhat like that in southern central Siberia existed. This premise is also supported by the fire ecology characteristics of the dominant vegetation. *Larix* does not support crown fires due to leaf moisture content (de Groot et al., 2013) and self-pruning (Kobayashi et al., 2007). The persistence and success of larch in modern-day Siberia appears to be driven by its high growth rate (Jacquelyn et al., 2017) tolerance of frequent surface fire due to thick lower bark (Kobayashi et al., 2007) and tolerance of spring drought due to its deciduous habit (Berg and Chapin III, 1994). Arboreal *Betula* are very intolerant of fire and easily girdled. However, they are quick to resprout and are often found in areas with short fire return intervals. Like *Larix*, arboreal *Betula* have high moisture content of their foliage and are not prone to crown fires. *Betula* nana L., an extant dwarf birch, is a fire endurer that resprouts from underground rhizomes or roots (Racine et al., 1987) thus regenerating quickly following lower severity fires (de Groot et al., 1997). The vegetation and fire regime characteristics are similar further up the sequence at 301.10-301.25 MASL, with the exception that ferns increased in abundance while heath decreased.

In the upper part of the sequence (301.35-301.45 MASL), where charcoal was abundant, the *Larix-Betula* parkland was replaced by a mixed boreal forest assemblage with a fern understory. Canopy cover was more closed compared to the preceding intervals. The forest was dominated by *Larix* and *Picea*, with lesser amounts of *Pinus*. While *Betula* remained part of the forest, it decreased in abundance possibly due to increased competition with the conifers. Based on exploratory CRACLE analyses of climate preferences using GBIF occurrence data (GBIF.org, 2018a, b, c, d) of the dominant taxa (*Larix-Betula* vs. *Larix-Picea-Pinus*), the expansion of conifers could indicate slightly warmer summers (MST ~15.8 ºC vs. 17.1 ºC). This result differs from the stable MST estimated by bacterial tetraethers, although within reported error, and the small change is certainly within the climate distributions of both communities. The analyses also suggest that slightly drier conditions may have prevailed during the three wettest months (249-285mm vs. 192-219mm). While the interaction between climate, vegetation and fire is complex, small changes is MST and precipitation could have directly altered both the vegetation and fire regime, which in turn further promoted fire adapted taxa. In addition to regional climatic factors, community change at the site may have been further influenced by local hydrological conditions, such as channel migration, pond infilling and ecosystem engineering by beaver (*Cantor spp*.).

The high charcoal content of the upper portion (~ Unit IV) of the sequence has three potential explanations: reworking of previously deposited charcoal, decreased sedimentation, or increased wildfire production of charcoal. We consider the first unlikely because there is no difference in the shape of the macrocharcoal between the upper and lower portions of the sequence, whereas we would anticipate a change in the dimensions of the charcoal if it had undergone additional physical breakdown from reworking (see Fig. S5). The second, decreased sedimentation, may occur if the deposition is a result of infrequent, episodic flooding intermixed with long periods during which charcoal

was deposited. The recorded sedimentology does not support this explanation, but due to the complexity of flooding processes, also does not disprove this explanation. We, however, favour the third explanation of increased wildfire due to the change in plant composition consistent with a greater influence of fire. If excepted, it is likely that frequent, mixed severity fires persisted. While *Larix* is associated with surface fire, *Picea* and *Pinus* are adapted to higher intensity crown fires. A crown fire regime may have established as conifers expanded, altering fuel loads and flammability. For example, black spruce sheds highly flammable needles, its lower branches can act as fuel ladders facilitating crown fires (Kasischke et al., 2008), and it was previously tentatively identified at BP (Fletcher et al., 2017). While it has thin bark and shallow roots maladapted to survive fire (Auclair, 1985; Brown, 2008; Kasischke et al., 2008), it releases large numbers of seeds from semi-serotinous cones, leading to rapid re-establishment (Côté et al., 2003). The documentation of Onagraceae pollen at the top of the sequence could potentially reflect post-fire succession. For example, the species *Epilobium angustifolium* L. is an early-seral colonizer of disturbed (i.e. burnt) sites, pollinated by insects.

It appears that the *Larix-Betula* parkland dominated intervals correspond to the peat- and sand-stratigraphic Units II and III described by Mitchell et al. (2016), whereas the mixed boreal forest in the upper part of the sequence is contemporaneous with Unit IV, described as peat and peaty sand, coarsening upwards. While it is clear that the vegetation and fire regimes changed through time at this Arctic site, CO_2 and temperatures appear more stable, or at least to have no apparent trend. Thus, it is suggested that the fire regime at BP was primarily regulated by regional climate and vegetation, and perhaps additionally by changing local hydrological conditions. Regarding climate, MST remained high enough (> ~13.5ºC) throughout the sequence to allow for fire disturbance and the pollen suggests that temperatures may have marginally increased in the upper part of the sequence. Alternatively, other climate variables, such as the precipitation regime, or local hydrological change may have initiated the change in community. Up-sequence changes in vegetation undoubtedly influenced fine fuel loads and flammability. Indeed, the fire ecological characteristics of the vegetation are consistent with a regional surface fire regime yielding to a crown fire regime.

Betula and *Alnus*, which occurred earlier in the depositional sequence, are favored by beaver in foraging (Busher, 1996; Haarberg and Rosell, 2006; Jenkins, 1979). Moreover, the presence of sticks cut by beaver in Unit III reveals that beavers were indeed at the site, moistening the local land surface. The lack of beaver cut sticks and changes in sediment in Unit IV may indicate that the beavers abandoned the site, possibly in response to changes in vegetation (i.e. increased conifers and decreased *Betula*) limiting preferred forage or due to lateral channel migration, as evidenced by the coarsening upward sequence described by Mitchell et al. (2016). As a result, the local land surface may have become somewhat drier, contemporaneous with the change towards *Larix-Picea-Pinus* forest and a mixed severity fire regime.

Critically, the charcoal record suggests that there was substantial biomass burning that could have been a feedback mechanism amplifying or dampening warming during the Pliocene due to its prevalence through time, and the complex direct impacts on the surface radiative budget and direct and indirect effects on the top of the atmosphere radiative budget (Feng et al., 2016). Further investigation is warranted to better characterize the fire regime to improve accuracy of fire simulations in earth system models of Pliocene climate.

5. CONCLUSION

The record of CO_2 in keeping with upper estimates from the Pliocene supports the hypothesis that Pliocene Arctic terrestrial fossil localities probably represent periods of higher warmth that supported higher productivity. The novel temperature estimates presented here suggest that summer temperatures were considerably warmer during the Pliocene (~15.4°C) compared to modern day Eureka, Canada (~4.1°C; Fig. 2). This supports an increasing influence of arctic amplification of temperatures as CO_2 reaches and exceeds modern levels. Our reconstruction of the paleovegetation and ecology of this unique site on Ellesmere Island suggests an assemblage similar to forests of the western margins of North America and eastern Fennoscandia. The evidence of recurrent fire and concurrent changes in taxonomic composition suggests that fire played an active role in Pliocene Arctic forests, shaping the environment as it does in the boreal forest today. Evidence from fire in the modern boreal forest suggests that fire may have had direct and indirect impacts on Earth's radiative budget at high latitudes during the Pliocene. The net impact of the component process remains unknown and modelling experiments are needed to quantitatively investigate the effects of the kind of fire regime presented here, on the Pliocene High Arctic. Collectively, these reconstructions provide new insights into the paleoclimatology and paleoecology of the Canadian High Arctic, ~3.9 Ma.

Data Availability. The data generated and used in this analysis are available in the supplemental information associated with this article.

Sample Availability. Samples used in this analysis are curated by the Canadian Museum of Nature. Sample numbers used for each analysis are given in the supplemental information (Table S3 and S4).

Supplemental Link. To be provided by Copernicus Publishing

Author Contribution. Conceptualization: A.P.B. with modification by other authors; Methodology: A.P.B., J.G., J.S.S.D., K.J.B., T.F.; Formal analysis: All authors; Investigation: A.P.B., J.G., K.J.B., L.W., T.F.; Resources: A.P.B., J.G., J.S.S.D., K.J.B.; Data curation: A.P.B., J.G., K.J.B., L.W., T.F.; Writing—Original draft: All authors; Writing—Review and editing: All authors; Supervision: A.P.B., J.S.S.D., K.J.B., N.R.; Project administration: A.P.B., N.R., T.F.; Funding acquisition: A.P.B., J.G., J.S.S.D., K.J.B., N.R., T.F. (Definitions as per the CRediT Taxonomy)

Competing interests. The authors declare that they have no conflict of interest

Acknowledgements. This work was funded by NSF Polar Programs to A.P.B.; National Geographic Committee for Research and Exploration Grant (9912-16) and Endeavour Research Fellowship (5928-2017) to T.F.; National Geographic Explorer Grant (7902-05), NSERC Discovery Grant (312193), and The W. Garfield Weston Foundation grant to N.R.; student travel (N.R. supervised) was supported by the Northern Scientific Training Program (NSTP) from the government of Canada; an NSERC Discovery Grant (239961) with Northern Supplement (362148) to J.C.G; Natural Resources Canada (SO-03 PA 3.1 Forest Disturbances Wildland Fire) to K.J.B.; the European Research

Council under the European Union′s Seventh Framework Programme (FP7/2007-2013) / ERC grant agreement n ° [226600], and funding from the Netherlands Earth System Science Center (NESSC) through a gravitation grant (NWO 024.002.001) from the Dutch Ministry for Education, Culture and Science to J.S.S.D.

Alice Telka (Paleotec Services) identified and prepared macrofossil plants for the CO_2 analysis. We are also grateful to Nicholas Conder (Canadian Forest Service) who assisted with sample preparation for the vegetation/fire reconstruction. We also acknowledge the 2006, 2008, 2010 and 2012 field teams including D. Finney (Environment Canada), H. Larson (McGill University), M. Vavrek (McGill University), A. Dececchi (McGill University), W.T. Mitchell (Carleton University), R. Smith (University of Saskatchewan), and C. Schröder-Adams (Carleton University). The field research was supported by a paleontology permit from the Government of Nunavut, CLEY (D.R. Stenton, J. Ross) and with the permission of Qikiqtani Inuit Association, especially Grise Fiord (Nunavut). Logistic support was provided by the Polar Continental Shelf Program (M. Bergmann, B. Hyrcyk, B. Hough, M. Kristjanson, T. McConaghy, J. MacGregor and the PCSP team).

References

Abbot, D. S. and Tziperman, E.: Sea ice, high-latitude convection, and equable climates, Geophysical Research Letters, 35, 2008.

Auclair, A. N.: Postfire regeneration of plant and soil organic pools in a *Picea mariana–Cladonia stellaris* ecosystem, Canadian Journal of Forest Research, 15, 279–291, 1985.

Ballantyne, A. P., Axford, Y., Miller, G. H., Otto-Bliesner, B. L., Rosenbloom, N., and White, J. W.: The amplification of Arctic terrestrial surface temperatures by reduced sea-ice extent during the Pliocene, Palaeogeography, Palaeoclimatology, Palaeoecology, 386, 59–67, 2013.

Ballantyne, A. P., Greenwood, D. R., Sinninghe Damsté, J. S., Csank, A. Z., Eberle, J. J., and Rybczynski, N.: Significantly warmer Arctic surface temperatures during the Pliocene indicated by multiple independent proxies, Geology, 38, 603–606, 2010.

Ballantyne, A. P., Rybczynski, N., Baker, P. A., Harington, C. R., and White, D.: Pliocene Arctic temperature constraints from the growth rings and isotopic composition of fossil larch, Palaeogeography, Palaeoclimatology, Palaeoecology, 242, 188–200, 2006.

Bauska, T. K., Baggenstos, D., Brook, E. J., Mix, A. C., Marcott, S. A., Petrenko, V. V., Schaefer, H., Severinghaus, J. P., and Lee, J. E.: Carbon isotopes characterize rapid changes in atmospheric carbon dioxide during the last deglaciation, Proceedings of the National Academy of Sciences, 2016. 201513868, 2016.

Bendle, J. A., Weijers, J. W., Maslin, M. A., Sinninghe Damsté, J. S., Schouten, S., Hopmans, E. C., Boot, C. S., and Pancost, R. D.: Major changes in glacial and Holocene terrestrial temperatures and sources of organic carbon recorded in the Amazon fan by tetraether lipids, Geochemistry, Geophysics, Geosystems, 11, 2010.

Berg, E. E. and Chapin III, F. S.: Needle loss as a mechanism of winter drought avoidance in boreal conifers, Canadian Journal of Forest Research, 24, 1144–1148, 1994.

Bergeron, Y.: The influence of island and mainland lakeshore landscapes on boreal forest fire regimes, Ecology, 72, 1980–1992, 1991.

Bergeron, Y., Cyr, D., Drever, C. R., Flannigan, M., Gauthier, S., Kneeshaw, D., Lauzon, È., Leduc, A., Goff, H. L., Lesieur, D., and Logan, K.: Past, current, and future fire frequencies in Quebec's commercial forests: implications for the cumulative effects of harvesting and fire on age-class structure and natural disturbance-based management, Canadian Journal of Forest Research, 36, 2737–2744, 2006.

Bonan, G.: Ecological climatology: concepts and applications, Cambridge University Press, 2015.

Bouchard, M., Pothier, D., and Gauthier, S.: Fire return intervals and tree species succession in the North Shore region of eastern Quebec, Canadian Journal of Forest Research, 38, 1621–1633, 2008.

Brigham-Grette, J. and Carter, L. D.: Pliocene Marine Transgressions of Northern Alaska: Circumarctic Correlations and Paleoclimatic Interpretations, Arctic, 45, 74–89, 1992.

Brown, K. J. and Giesecke, T.: Holocene fire disturbance in the boreal forest of central Sweden, Boreas, 43, 639–651, 2014.

Brown, K. J. and Power, M. J.: Charred particle analyses. In: Encyclopedia of Quaternary Science, Elias, S. (Ed.), Elsevier, Amsterdam, 2013.

Brown, M.: Fire and Ice: Fire Severity and Future Flammability in Alaskan Black Spruce Forests, Fire Science Brief, 2008. 1–6, 2008.

Busher, P. E.: Food Caching Behavior of Beavers (*Castor canadensis*): Selection and Use of Woody Species, The American Midland Naturalist, 135, 343-348, 1996.

Clymo, R. S.: The Origin of Acidity in Sphagnum Bogs, The Bryologist, 67, 427–431, 1964.

Côté, M., Ferron, J., and Gagnon, R.: Impact of seed and seedling predation by small rodents on early regeneration establishment of black spruce, Canadian Journal of Forest Research, 33, 2362–2371, 2003.

Csank, A. Z., Patterson, W. P., Eglington, B. M., Rybczynski, N., and Basinger, J. F.: Climate variability in the Early Pliocene Arctic: Annually resolved evidence from stable isotope values of sub-fossil wood, Ellesmere Island, Canada, Palaeogeography, Palaeoclimatology, Palaeoecology, 308, 339–349, 2011a.

Csank, A. Z., Tripati, A. K., Patterson, W. P., Eagle, R. A., Rybczynski, N., Ballantyne, A. P., and Eiler, J. M.: Estimates of Arctic land surface temperatures during the early Pliocene from two novel proxies, Earth and Planetary Science Letters, 304, 291–299, 2011b.

de Groot, W. J., Cantin, A. S., Flannigan, M. D., Soja, A. J., Gowman, L. M., and Newbery, A.: A comparison of Canadian and Russian boreal forest fire regimes, Forest Ecology and Management, 294, 23–34, 2013.

de Groot, W. J., Thomas, P. A., and Wein, R. W.: *Betula nana* L. *and Betula glandulosa* Michx, Journal of Ecology, 85, 241–264, 1997.

De Jonge, C., Hopmans, E. C., Stadnitskaia, A., Rijpstra, W. I. C., Hofland, R., Tegelaar, E., and Sinninghe Damsté, J. S.: Identification of novel penta-and hexamethylated branched glycerol dialkyl glycerol tetraethers in peat using HPLC–MS 2, GC–MS and GC–SMB-MS, Organic geochemistry, 54, 78–82, 2013.

De Jonge, C., Hopmans, E. C., Zell, C. I., Kim, J.-H., Schouten, S., and Sinninghe Damsté, J. S.: Occurrence and abundance of 6-methyl branched glycerol dialkyl glycerol tetraethers in soils: Implications for palaeoclimate reconstruction, Geochimica et Cosmochimica Acta, 141, 97–112, 2014.

De Jonge, C., Stadnitskaia, A., Hopmans, E. C., Cherkashov, G., Fedotov, A., Streletskaya, I. D., Vasiliev, A. A., and Sinninghe Damsté, J. S.: Drastic changes in the distribution of branched tetraether lipids in suspended matter and sediments from the Yenisei River and Kara Sea (Siberia): Implications for the use of brGDGT-based proxies in coastal marine sediments, Geochimica et Cosmochimica Acta, 165, 200–225, 2015.

de Lafontaine, G. and Payette, S.: Shifting zonal patterns of the southern boreal forest in eastern Canada associated with changing fire regime during the Holocene, Quaternary Science Reviews, 30, 867–875, 2011.

Dee, D. P., Uppala, S. M., Simmons, A. J., Berrisford, P., Poli, P., Kobayashi, S., Andrae, U., Balmaseda, M. A., Balsamo, G., and Bauer, P.: The ERA-Interim reanalysis: Configuration and performance of the data assimilation system, Quarterly Journal of the Royal Meteorological Society, 137, 553–597, 2011.

Diefendorf, A. F., Mueller, K. E., Wing, S. L., Koch, P. L. and Freeman, K. H..:Global patterns in leaf 13C discrimination and implications for studies of past and future climate. *Proceedings of the National Academy of Sciences,* 107, 5738-5743. 2010

Dowsett, H., Dolan, A., Rowley, D., Pound, M., Salzmann, U., Robinson, M., Chandler, M., Foley, K., and Haywood, A.: The PRISM4 (mid-Piacenzian) palaeoenvironmental reconstruction, Climate of the Past, doi: doi:10.5194/cp-12-1519-2016, 2016. 2016.

Dowsett, H. J., Cronin, T. M., Poore, R. Z., Thompson, R. S., Whatley, R. C., and Wood, A. M.: Micropaleontological evidence for increased meridional heat transport in the North Atlantic Ocean during the Pliocene, Science, 258, 1133–1136, 1992.

Dowsett, H. J., Robinson, M. M., Haywood, A. M., Hill, D. J., Dolan, A. M., Stoll, D. K., Chan, W. L., Abe-Ouchi, A., Chandler, M. A., and Rosenbloom, N. A.: Assessing confidence in Pliocene sea surface temperatures to evaluate predictive models, Nature Climate Change, 2, 365–371, 2012.

Estrada, S., Piepjohn, K., Frey, M. J., Reinhardt, L., Andruleit, H., and von Gosen, W.: Pliocene coal-seam fires on southern Ellesmere Island, Canadian Arctic, Neues Jahrbuch für Geologie und Paläontologie - Abhandlungen, 251, 33-52, 2009.

Farquhar, G. D., Ehleringer, J. R., and Hubick, K. T.: Carbon isotope discrimination and photosynthesis, Annual Review of Plant Biology, 40, 503–537, 1989.

Feng, R., Otto-Bliesner, B., Fletcher, T., Ballantyne, A., and Brady, E.: Contributions to Pliocene Arctic warmth from removal of anthropogenic aerosol and enhanced forest fire emissions, San Francisco, USA. 2016, PP33A-2344.

Feng, R., Otto-Bliesner, B. L., Fletcher, T. L., Tabor, C. R., Ballantyne, A. P., and Brady, E. C.: Amplified Late Pliocene terrestrial warmth in northern high latitudes from greater radiative forcing and closed Arctic Ocean gateways, Earth and Planetary Science Letters, 466, 129-138, 2017.

Flannigan, M., Stocks, B., Turetsky, M., and Wotton, M.: Impacts of climate change on fire activity and fire management in the circumboreal forest, Global Change Biology, 15, 549–560, 2009.

Fletcher, B. J., Brentnall, S. J., Anderson, C. W., Berner, R. A., and Beerling, D. J.: Atmospheric carbon dioxide linked with Mesozoic and early Cenozoic climate change, Nature Geoscience, 1, 43–48, 2008.

Fletcher, T., Feng, R., Telka, A. M., Matthews, J. V., and Ballantyne, A.: Floral dissimilarity and the influence of climate in the Pliocene High Arctic: Biotic and abiotic influences on five sites on the Canadian Arctic Archipelago, Frontiers in Ecology and Evolution, 5, 19, 2017.

Foster, L. C., Pearson, E. J., Juggins, S., Hodgson, D. A., Saunders, K. M., Verleyen, E., and Roberts, S. J.: Development of a regional glycerol dialkyl glycerol tetraether (GDGT)–temperature calibration for Antarctic and sub-Antarctic lakes, Earth and Planetary Science Letters, 433, 370–379, 2016.

Foster, G. L., Royer, D. L., and Lunt, D. J.: Future climate forcing potentially without precedent in the last 420 million years, Nature Communications, 8, 14845, 2017.

Francis, J. and Skific, N.: Evidence linking rapid Arctic warming to mid-latitude weather patterns, Philosophical Transactions of the Royal Society A: Mathematical, Physical and Engineering Sciences, 373, 1–12, 2015.

GBIF.org: GBIF Occurrence Download (Beaver Pond extant species) http://doi.org/10.15468/dl.ertiqj 1st February 2017.

GBIF.org: GBIF Occurrence Download (*Betula*) https://doi.org/10.15468/dl.akxgp5 11th May 2018a.

GBIF.org: GBIF Occurrence Download (*Larix*) https://doi.org/10.15468/dl.mfhnci 11th May 2018b.

GBIF.org: GBIF Occurrence Download (*Picea*) https://doi.org/10.15468/dl.wi7jdc 11th May 2018c.

GBIF.org: GBIF Occurrence Download (*Pinus*) https://doi.org/10.15468/dl.vwfjj2 11th May 2018d.

Global View-CO_2: Cooperative Global Atmospheric Data Integration Project. 2013, updated annually. Multi-laboratory compilation of synchronized and gap-filled atmospheric carbon dioxide records for the period 1979-2012. Compiled by NOAA Global Monitoring Division: Boulder, Colorado, U.S.A, 2013.

Greene, G. A. and Daniels, L. D.: Spatial interpolation and mean fire interval analyses quantify historical mixed-severity fire regimes, International Journal of Wildland Fire, 26, 136–147, 2017.

Haarberg, O. and Rosell, F.: Selective foraging on woody plant species by the Eurasian beaver (*Castor fiber*) in Telemark, Norway, Journal of Zoology, 270, 201-208, 2006.

Haywood, A. M., Dowsett, H. J., and Dolan, A. M.: Integrating geological archives and climate models for the mid-Pliocene warm period, Nature communications, 7, 1-14, 2016.

Higuera, P., Barnes, J. L., Chipman, M. L., Urban, M., and Hu, F. S.: The burning tundra: A look back at the last 6,000 years of fire in the Noatak National Preserve, Northwestern Alaska, Alaska Park Science, 10, 37–41, 2011.

Higuera, P. E., Brubaker, L. B., Anderson, P. M., Hu, F. S., and Brown, T. A.: Vegetation mediated the impacts of postglacial climate change on fire regimes in the south-central Brooks Range, Alaska, Ecological Monographs, 79, 201–219, 2009.

Hijmans, R. J., Cameron, S. E., Parra, J. L., Jones, P. G., and Jarvis, A.: Very high resolution interpolated climate surfaces for global land areas, International Journal of Climatology, 25, 1965–1978, 2005.

Hönisch, B., Hemming, N. G., Archer, D., Siddall, M., and McManus, J. F.: Atmospheric Carbon Dioxide Concentration Across the Mid-Pleistocene Transition, Science, 324, 1551-1554, 2009.

Hopmans, E. C., Schouten, S., and Sinninghe Damsté, J. S.: The effect of improved chromatography on GDGT-based palaeoproxies, Organic Geochemistry, 93, 1–6, 2016.

Hu, F. S., Higuera, P. E., Walsh, J. E., Chapman, W. L., Duffy, P. A., Brubaker, L. B., and Chipman, M. L.: Tundra burning in Alaska: Linkages to climatic change and sea ice retreat, Journal of Geophysical Research: Biogeosciences, 115, 2010.

Huber, M.: A Hotter Greenhouse?, Science, 321, 353–354, 2008.

Huguet, C., Hopmans, E. C., Febo-Ayala, W., Thompson, D. H., Sinninghe Damsté, J. S., and Schouten, S.: An improved method to determine the absolute abundance of glycerol dibiphytanyl glycerol tetraether lipids, Organic Geochemistry, 37, 1036–1041, 2006.

Hwang, Y. T., Frierson, D. M., and Kay, J. E.: Coupling between Arctic feedbacks and changes in poleward energy transport, Geophysical Research Letters, 38, 2011.

Jacquelyn, K. S., Adrianna, C. F., Herman, H. S., Amanda, H.-H., Alexander, K., Tatiana, L., Dmitry, E., and Elena, S.: Fire disturbance and climate change: implications for Russian forests, Environmental Research Letters, 12, 035003, 2017.

Jenkins, S. H.: Seasonal and year-to-year differences in food selection by beavers, Oecologia, 44, 112-116, 1979.

Johnstone, J. F., Chapin, F. S., Hollingsworth, T. N., Mack, M. C., Romanovsky, V., and Turetsky, M.: Fire, climate change, and forest resilience in interior Alaska, Canadian Journal of Forest Research, 40, 1302–1312, 2010a.

Johnstone, J. F., Hollingsworth, T. N., Chapin, F. S., and Mack, M. C.: Changes in fire regime break the legacy lock on successional trajectories in Alaskan boreal forest, Global Change Biology, 16, 1281–1295, 2010b.

Johnstone, J. F. and Kasischke, E. S.: Stand-level effects of soil burn severity on postfire regeneration in a recently burned black spruce forest, Canadian Journal of Forest Research, 35, 2151–2163, 2005.

Jones, P. D. and Moberg, A.: Hemispheric and large-scale surface air temperature variations: An extensive revision and an update to 2001, Journal of Climate, 16, 206–223, 2003.

Kasischke, E. S. and Turetsky, M. R.: Recent changes in the fire regime across the North American boreal region—spatial and temporal patterns of burning across Canada and Alaska, Geophysical research letters, 33, 2006.

Kasischke, E. S., Turetsky, M. R., Ottmar, R. D., French, N. H., Hoy, E. E., and Kane, E. S.: Evaluation of the composite burn index for assessing fire severity in Alaskan black spruce forests, International Journal of Wildland Fire, 17, 515–526, 2008.

Kasischke, E. S., Williams, D., and Barry, D.: Analysis of the patterns of large fires in the boreal forest region of Alaska, International Journal of Wildland Fire, 11, 131–144, 2002.

Kharuk, V. I., Dvinskaya, M. L., Petrov, I. A., Im, S. T., and Ranson, K. J.: Larch forests of Middle Siberia: long-term trends in fire return intervals, Regional Environmental Change, doi: 10.1007/s10113-016-0964-9, 2016. 1–9, 2016.

Kharuk, V. I., Ranson, K. J., Dvinskaya, M. L., and Im, S. T.: Wildfires in northern Siberian larch dominated communities, Environmental Research Letters, 6, 045208, 2011.

Kobayashi, M., Nemilostiv, Y. P., Zyryanova, O. A., Kajimoto, T., Matsuura, Y., Yoshida, T., Satoh, F., Sasa, K., and Koike, T.: Regeneration after forest fires in mixed conifer broad-leaved forests of the Amur region in far eastern Russia: the relationship between species specific traits against fire and recent fire regimes, Eurasian Journal of Forest Research, 10, 51–58, 2007.

Kooijman, A. and Westhoff, V.: Variation in habitat factors and species composition of *Scorpidium scorpioides* communities in NW-Europe, Plant Ecology, 117, 133–150, 1995.

Kooijman, A. M. and Paulissen, M. P. C. P.: Higher acidification rates in fens with phosphorus enrichment, Applied Vegetation Science, 9, 205–212, 2006.

Leavitt, S. W. and Danzer, S. R.: Method for batch processing small wood samples to holocellulose for stable-carbon isotope analysis, Analytical Chemistry, 65, 87–89, 1993.

Lifton, N., Sato, T., and Dunai, T. J.: Scaling in situ cosmogenic nuclide production rates using analytical approximations to atmospheric cosmic-ray fluxes, Earth and Planetary Science Letters, 386, 149–160, 2014.

Lisiecki, L. E. and Raymo, M. E.: A Plio-Pleistocene stack of 57 globally distributed benthic $\delta^{18}O$ records, Paleoceanography, 20, 2005.

Loomis, S. E., Russell, J. M., Ladd, B., Street-Perrott, F. A., and Sinninghe Damsté, J. S.: Calibration and application of the branched GDGT temperature proxy on East African lake sediments, Earth and Planetary Science Letters, 357, 277–288, 2012.

Lorimer, C. G.: The Presettlement Forest and Natural Disturbance Cycle of Northeastern Maine, Ecology, 58, 139–148, 1977.

Luthi, D., Le Floch, M., Bereiter, B., Blunier, T., Barnola, J.-M., Siegenthaler, U., Raynaud, D., Jouzel, J., Fischer, H., Kawamura, K., and Stocker, T. F.: High-resolution carbon dioxide concentration record 650,000-800,000 years before present, Nature, 453, 379–382, 2008.

Lynch, J. A., Clark, J. S., Bigelow, N. H., Edwards, M. E., and Finney, B. P.: Geographic and temporal variations in fire history in boreal ecosystems of Alaska, Journal of Geophysical Research: Atmospheres, 107, FFR 8-1–FFR 8-17, 2002.

Mack, M. C., Bret-Harte, M. S., Hollingsworth, T. N., Jandt, R. R., Schuur, E. A. G., Shaver, G. R., and Verbyla, D. L.: Carbon loss from an unprecedented Arctic tundra wildfire, Nature, 475, 489–492, 2011.

Marshall, J., Armour, K. C., Scott, J. R., Kostov, Y., Hausmann, U., Ferreira, D., Shepherd, T. G., and Bitz, C. M.: The ocean's role in polar climate change: asymmetric Arctic and Antarctic responses to greenhouse gas and ozone forcing, Philosophical Transactions of the Royal Society of London A: Mathematical, Physical and Engineering Sciences, 372, 20130040, 2014.

Martinez-Boti, M. A., Foster, G. L., Chalk, T. B., Rohling, E. J., Sexton, P. F., Lunt, D. J., Pancost, R. D., Badger, M. P. S., and Schmidt, D. N.: Plio-Pleistocene climate sensitivity evaluated using high-resolution CO_2 records, Nature, 518, 49–54, 2015.

Matthews Jr, J. V. and Ovenden, L. E.: Late Tertiary plant macrofossils from localities in Arctic/sub- Arctic North America: a review of the data, Arctic, 43, 364–392, 1990.

Matthews, J. V. J. and Fyles, J. G.: Late Tertiary plant and arthropod fossils from the High Terrace Sediments on the Fosheim Peninsula of Ellesmere Island (Northwest Territories, District of Franklin), Geological Survey of Canada, Bulletin, 529, 295–317, 2000.

Mattson, M. D.: Acid lakes and rivers. In: Environmental Geology, Springer Netherlands, Dordrecht, 1999.

McAndrews, J. H., Berti, A. A., and Norris, G.: Key to the Quaternary pollen and spores of the Great Lakes region, 1973. 1973.

Ménot, G. and Burns, S. J.: Carbon isotopes in ombrogenic peat bog plants as climatic indicators: calibration from an altitudinal transect in Switzerland, Organic Geochemistry, 32, 233–245, 2001.

Miller, G. H., Alley, R. B., Brigham-Grette, J., Fitzpatrick, J. J., Polyak, L., Serreze, M. C., and White, J. W. C.: Arctic amplification: can the past constrain the future?, Quaternary Science Reviews, 29, 1779–1790, 2010.

Mitchell, W. T., Rybczynski, N., Schröder-Adams, C., Hamilton, P. B., Smith, R., and Douglas, M.: Stratigraphic and Paleoenvironmental Reconstruction of a Mid-Pliocene Fossil Site in the High Arctic (Ellesmere Island, Nunavut): Evidence of an Ancient Peatland with Beaver Activity, Arctic, 69, 185–204, 2016.

Moore, P. D., Webb, J. A., and Collison, M. E.: Pollen analysis, Blackwell Scientific Publications, Oxford, 1991.

Naafs, B., Inglis, G., Zheng, Y., Amesbury, M., Biester, H., Bindler, R., Blewett, J., Burrows, M., del Castillo Torres, D., and Chambers, F. M.: Introducing global peat-specific temperature and pH calibrations based on brGDGT bacterial lipids, Geochimica et Cosmochimica Acta, 208, 285–301, 2017.

Niemann, H., Stadtnitskaia, A., Wirth, S., Gilli, A., Anselmetti, F., Sinninghe Damsté, J., Schouten, S., Hopmans, E., and Lehmann, M.: Bacterial GDGTs in Holocene sediments and catchment soils of a high Alpine lake: application of the MBT/CBT-paleothermometer, Climate of the Past, 8, 889-906, 2012.

Niklasson, M. and Drakenberg, B.: A 600-year tree-ring fire history from Norra Kvills National Park, southern Sweden: implications for conservation strategies in the hemiboreal zone, Biological Conservation, 101, 63–71, 2001.

Niklasson, M. and Granström, A.: Fire in Sweden – History, Research, Prescribed Burning and Forest Certification, International Forest Fire News, 30, 80–83, 2004.

Niklasson, M. and Granström, A.: Numbers and sizes of fires: Long-term spatially explicit fire history in a Swedish boreal landscape, Ecology, 81, 1484–1499, 2000.

Otto-Bliesner, B. L. and Upchurch Jr, G. R.: Vegetation-induced warming of high-latitude regions during the Late Cretaceous period, Nature, 385, 804, 1997.

Pagani, M., Liu, Z., LaRiviere, J., and Ravelo, A. C.: High Earth-system climate sensitivity determined from Pliocene carbon dioxide concentrations, Nature Geoscience, 3, 27–30, 2010.

Pearson, E. J., Juggins, S., Talbot, H. M., Weckström, J., Rosén, P., Ryves, D. B., Roberts, S. J., and Schmidt, R.: A lacustrine GDGT-temperature calibration from the Scandinavian Arctic to Antarctic: Renewed potential for the application of GDGT-paleothermometry in lakes, Geochimica et Cosmochimica Acta, 75, 6225–6238, 2011.

Peterse, F., Prins, M. A., Beets, C. J., Troelstra, S. R., Zheng, H., Gu, Z., Schouten, S., and Sinninghe Damsté, J. S.: Decoupled warming and monsoon precipitation in East Asia over the last deglaciation, Earth and Planetary Science Letters, 301, 256–264, 2011.

Powers, L. A., Werne, J. P., Johnson, T. C., Hopmans, E. C., Sinninghe Damsté, J. S., and Schouten, S.: Crenarchaeotal membrane lipids in lake sediments: A new paleotemperature proxy for continental paleoclimate reconstruction?, Geology, 32, 613–616, 2004.

R Core Team: R: A language and environment for statistical computing. R Foundation for Statistical Computing, Vienna, Austria, 2016.

Racine, C. H., Johnson, L. A., and Viereck, L. A.: Patterns of Vegetation Recovery after Tundra Fires in Northwestern Alaska, U.S.A, Arctic and Alpine Research, 19, 461–469, 1987.

Ravelo, A. C., Andreasen, D. H., Lyle, M., Lyle, A. O., and Wara, M. W.: Regional climate shifts caused by gradual global cooling in the Pliocene epoch, Nature, 429, 263-267, 2004.

Raymo, M. E., Lisiecki, L. E., and Nisancioglu, K. H.: Plio-Pleistocene ice volume, Antarctic climate, and the global $\delta^{18}O$ record, Science, 313, 492-495, 2006.

Robinson, M. M.: New Quantitative Evidence of Extreme Warmth in the Pliocene Arctic, Stratigraphy, 6, 265–275, 2009.

Rogers, B. M., Soja, A. J., Goulden, M. L., and Randerson, J. T.: Influence of tree species on continental differences in boreal fires and climate feedbacks, Nature Geoscience, 8, 228–234, 2015.

Rovere, A., Raymo, M. E., Mitrovica, J. X., Hearty, P. J., O'Leary, M. J., and Inglis, J. D.: The Mid-Pliocene sea-level conundrum: Glacial isostasy, eustasy and dynamic topography, Earth and Planetary Science Letters, 387, 27–33, 2014.

Royer, D. L.: CO 2-forced climate thresholds during the Phanerozoic, Geochimica et Cosmochimica Acta, 70, 5665-5675, 2006.

Royer, D. L., Berner, R. A., and Park, J.: Climate sensitivity constrained by CO_2 concentrations over the past 420 million years, Nature, 446, 530-532, 2007.

Royles, J., Horwath, A. B., and Griffiths, H.: Interpreting bryophyte stable carbon isotope composition: Plants as temporal and spatial climate recorders, Geochemistry, Geophysics, Geosystems, 15, 1462–1475, 2014.

Russell, J. M., Hopmans, E. C., Loomis, S. E., Liang, J., and Sinninghe Damsté, J. S.: Distributions of 5- and 6-methyl branched glycerol dialkyl glycerol tetraethers (brGDGTs) in East African lake sediment: Effects of temperature, pH, and new lacustrine paleotemperature calibrations, Geochimica et Cosmochimica Acta, 117, 56–69, 2018.

Ryan, K. C.: Dynamic interactions between forest structure and fire behavior in boreal ecosystems, Silva Fennica, 36, 13–39, 2002.

Rybczynski, N., Gosse, J. C., Richard Harington, C., Wogelius, R. A., Hidy, A. J., and Buckley, M.: Mid-Pliocene warm-period deposits in the High Arctic yield insight into camel evolution, Nature Communications, 4, 1–9, 2013.

Salzmann, U., Dolan, A. M., Haywood, A. M., Chan, W.-L., Voss, J., Hill, D. J., Abe-Ouchi, A., Otto-Bliesner, B., Bragg, F. J., and Chandler, M. A.: Challenges in quantifying Pliocene terrestrial warming revealed by data-model discord, Nature Climate Change, 3, 969, 2013.

Salzmann, U., Haywood, A. M., Lunt, D., Valdes, P., and Hill, D.: A new global biome reconstruction and data-model comparison for the middle Pliocene, Global Ecology and Biogeography, 17, 432–447, 2008.

Schlesinger, W. H. and Vengosh, A.: Global boron cycle in the Anthropocene, Global Biogeochemical Cycles, 30, 219–230, 2016.

Seki, O., Foster, G. L., Schmidt, D. N., Mackensen, A., Kawamura, K., and Pancost, R. D.: Alkenone and boron-based Pliocene pCO_2 records, Earth and Planetary Science Letters, 292, 201–211, 2010.

Shellito, C. J., Lamarque, J.-F. o., and Sloan, L. C.: Early Eocene Arctic climate sensitivity to pCO_2 and basin geography, Geophysical Research Letters, 36, 2009.

Sinninghe Damsté, J. S.: Spatial heterogeneity of sources of branched tetraethers in shelf systems: The geochemistry of tetraethers in the Berau River delta (Kalimantan, Indonesia), Geochimica et Cosmochimica Acta, 186, 13–31, 2016.

Sinninghe Damsté J.S., Rijpstra W.I.C., Foesel B.U., Huber K., Overmann J., Nakagawa S., Joong Jae Kim, Dunfield P.F. Dedysh S.N., Villanueva L. (2018) An overview of the occurrence of ether- and ester-linked iso-diabolic acid membrane lipids in microbial cultures of the Acidobacteria: Implications for brGDGT palaeoproxies for temperature and pH. Organic Geochemistry, 124, 63–76.

Sinninghe Damsté, J. S., Rijpstra, W. I. C., Hopmans, E. C., Foesel, B. U., Wüst, P. K., Overmann, J., Tank, M., Bryant, D. A., Dunfield, P. F., Houghton, K., and Stott, M. B.: Ether- and Ester-Bound iso-Diabolic Acid and Other Lipids in Members of Acidobacteria Subdivision 4, Applied and Environmental Microbiology, 80, 5207–5218, 2014.

Sinninghe Damsté, J. S., Rijpstra, W. I. C., Hopmans, E. C., Weijers, J. W., Foesel, B. U., Overmann, J., and Dedysh, S. N.: 13, 16-Dimethyl octacosanedioic acid (iso-diabolic acid), a common membrane-spanning lipid of Acidobacteria subdivisions 1 and 3, Applied and Environmental Microbiology, 77, 4147–4154, 2011.

Skrzypek, G., Kałużny, A., Wojtuń, B., and Jędrysek, M.-O.: The carbon stable isotopic composition of mosses: A record of temperature variation, Organic Geochemistry, 38, 1770–1781, 2007.

Stap, L. B., de Boer, B., Ziegler, M., Bintanja, R., Lourens, L. J., and van de Wal, R. S.: CO_2 over the past 5 million years: Continuous simulation and new δ11B-based proxy data, Earth and Planetary Science Letters, 439, 1–10, 2016.

Swann, A. L., Fung, I. Y., Levis, S., Bonan, G. B., and Doney, S. C.: Changes in Arctic vegetation amplify high-latitude warming through the greenhouse effect, Proceedings of the National Academy of Sciences of the United States of America, 107, 1295-1300, 2010.

Tedford, R. H. and Harington, C. R.: An Arctic mammal fauna from the early Pliocene of North America, Nature, 425, 388–390, 2003.

Tripati, A. K., Roberts, C. D., and Eagle, R. A.: Coupling of CO2 and Ice Sheet Stability over Major Climate Transitions of the Last 20 Million Years, Science, 326, 1394–1397, 2009.

Van Wagner, C. E., Finney, M. A., and Heathcott, M.: Historical fire cycles in the Canadian Rocky Mountain parks, Forest Science, 52, 704-717, 2006.

Waite, M. and Sack, L.: Shifts in bryophyte carbon isotope ratio across an elevation× soil age matrix on Mauna Loa, Hawaii: do bryophytes behave like vascular plants?, Oecologia, 166, 11–22, 2011.

Wang, X., Rybczynski, N., Harington, C. R., White, S. C., and Tedford, R. H.: A basal ursine bear (*Protarctos abstrusus*) from the Pliocene High Arctic reveals Eurasian affinities and a diet rich in fermentable sugars, Scientific reports, 7, 17722, 2017.

Warden, L., Jung-Hyun, K., Zell, C., Vis, G.-J., de Stigter, H., Bonnin, J., and Sinninghe Damsté, J. S.: Examining the provenance of branched GDGTs in the Tagus River drainage basin and its outflow into the Atlantic Ocean over the Holocene to determine their usefulness for paleoclimate applications, Biogeosciences, 13, 5719, 2016.

Weijers, J. W., Schefuß, E., Schouten, S., and Sinninghe Damsté, J. S.: Coupled thermal and hydrological evolution of tropical Africa over the last deglaciation, Science, 315, 1701–1704, 2007a.

Weijers, J. W., Schouten, S., van den Donker, J. C., Hopmans, E. C., and Sinninghe Damsté, J. S.: Environmental controls on bacterial tetraether membrane lipid distribution in soils, Geochimica et Cosmochimica Acta, 71, 703-713, 2007b.

Weijers, J. W. H., Schouten, S., van den Donker, J. C., Hopmans, E. C., and Sinninghe Damsté, J. S.: Environmental controls on bacterial tetraether membrane lipid distribution in soils, Geochimica et Cosmochimica Acta, 71, 703-713, 2007c.

White, J., Ciais, P., Figge, R., Kenny, R., and Markgraf, V.: A high-resolution record of atmospheric CO_2 content from carbon isotopes in peat, Nature, 367, 153–156, 1994.

Whitman, E., Batllori, E., Parisien, M. A., Miller, C., Coop, J. D., Krawchuk, M. A., Chong, G. W., and Haire, S. L.: The climate space of fire regimes in north-western North America, Journal of Biogeography, 42, 1736–1749, 2015.

Wright, C. S. and Agee, J. K.: Fire and vegetation history in the eastern Cascade Mountains, Washington, Ecological Applications, 14, 443–459, 2004.

Yang, G., Zhang, C. L., Xie, S., Chen, Z., Gao, M., Ge, Z., and Yang, Z.: Microbial glycerol dialkyl glycerol tetraethers from river water and soil near the Three Gorges Dam on the Yangtze River, Organic Geochemistry, 56, 40–50, 2013.

Yarie, J.: Forest fire cycles and life tables: a case study from interior Alaska, Canadian Journal of Forest Research, 11, 554–562, 1981.

Young, A. M., Higuera, P. E., Duffy, P. A., and Hu, F. S.: Climatic thresholds shape northern high-latitude fire regimes and imply vulnerability to future climate change, Ecography, 40, 606–617, 2017.

Zech, R., Gao, L., Tarozo, R., and Huang, Y.: Branched glycerol dialkyl glycerol tetraethers in Pleistocene loess-paleosol sequences: three case studies, Organic geochemistry, 53, 38–44, 2012.

Zell, C., Kim, J.-H., Moreira-Turcq, P., Abril, G., Hopmans, E. C., Bonnet, M.-P., Sobrinho, R. L., and Sinninghe Damsté, J. S.: Disentangling the origins of branched tetraether lipids and crenarchaeol in the lower Amazon River: Implications for GDGT-based proxies, Limnology and Oceanography, 58, 343–353, 2013.

Zhu, C., Weijers, J. W., Wagner, T., Pan, J.-M., Chen, J.-F., and Pancost, R. D.: Sources and distributions of tetraether lipids in surface sediments across a large river-dominated continental margin, Organic Geochemistry, 42, 376–386, 2011.

Zink, K.-G., Vandergoes, M. J., Mangelsdorf, K., Dieffenbacher-Krall, A. C., and Schwark, L.: Application of bacterial glycerol dialkyl glycerol tetraethers (GDGTs) to develop modern and past temperature estimates from New Zealand lakes, Organic Geochemistry, 41, 1060–1066, 2010.

1041 **Table 1. Modern and recent Holocene fire return interval reconstructions for the candidate analogous regions considered**
1042 **in this study.**

Region	Modern		Reference	Recent Holocene		Reference
Alaskan Tundra	Seward Peninsula	273*	Kasischke et al. (2002)	Up-Valley	263	Higuera et al. (2011)
	Nulato Hills	306*		Down-valley	142	
Alaskan Boreal	Porcupine/ Upper Yukon (Central)	~100	Yarie (1981)			
	Sites near Fairbanks, and Delta Junction (Central)	70130	Johnstone et al. (2010a); Johnstone et al. (2010b); Johnstone and Kasischke (2005)			
	Kenai Peninsula		Lynch et al. (2002)	Interior Alaska and Kenai Peninsula	198 ± 90	Lynch et al. (2002)
	Yukon river Lowlands	120	Kasischke et al. (2002)	Brooks Range	145	Higuera et al. (2009)
	Kuskokwim Mountains	218				
	Yukon-Tanama Uplands	330				
	Tanana-Kuskokwim Lowlands	178				
	Kobuk Ridges and Valleys	175				
	Davidson Mountains	403				
	North Ogilive Mountains	112				
	Ray Mountains	109				
	Yukon-Old Crow Basin	81				

Western North America	Darkwoods, British Columbia	~69	Greene and Daniels (2017)			
	Cascade Mountains, Washington	~27	Wright and Agee (2004)			
	Desolation Peak, Washington Coastal type	108-137				
	Desolation Peak, Washington Interior type	~52				
Eastern North America	Quebec – west	~270*	Bouchard et al. (2008)	Maine	≥ 800	Lorimer (1977)
	Quebec – east	>500*				
				Quebec – "Spruce zone"	570	de Lafontaine and Payette (2011)
				Quebec – "Fir zone"	>1000	
	Quebec – Abitibi northwest	418*	Bergeron et al. (2006 post-1940)^	Quebec – Abitibi northwest	189	Bergeron et al. (2006 post-1940)^
	Quebec – Abitibi southwest	388*		Quebec – Abitibi southwest	165	
	Quebec – Abitibi east	418*		Quebec – Abitibi east	141	
	Quebec – Abitibi southeast	2083*		Quebec – Abitibi southeast	257	
	Quebec – Temiscamingue north	2083*		Quebec – Temiscamingue north	220	

	Quebec – Temiscamingue south	2777*		Quebec – Temiscamingue south	313	
	Quebec – Waswanipi	418*		Quebec – Waswanipi	128	
	Quebec – Central Quebec	388*		Quebec – Central Quebec	150	
	Quebec – North Shore	645*		Quebec – North Shore	281	
	Quebec – Gaspésia	488*		Quebec – Gaspésia	161	
	Quebec – northwestern - lakeshore	99’	Bergeron (1991)	Quebec – northwestern - lakeshore	63’	Bergeron (1991)
	Quebec – northwestern – lake island	112’		Quebec – northwestern – lake island	74’	
Fennoscandia	Sweden	*	Niklasson and Drakenberg (2001); Niklasson and Granström (2004)	North Sweden	50-150	Niklasson and Granström (2004); Niklasson and Granström (2000)
				Southern Sweden	20	Niklasson and Drakenberg (2001)
	Central Sweden	*	Brown and Giesecke (2014)	Central Sweden - Klotjärnen	180	Brown and Giesecke (2014)
				Central Sweden - Holtjärnen	240	
Siberian Plateau	Northern	300	Kharuk et al. (2016); Kharuk et al. (2011)			
	Southern	80				
	Mean (64-71°N)	110				

^ = The reciprocal converted from burn rate (%) (see Van Wagner et al., 2006)

* = Estimates likely effected in some areas by human activity. In such instances Recent Holocene is preferred.

‘ = Fire cycle

†=‘Recent’ here refers to records that (or have distinct sections that) begin after the end of the Holocene Climate Optima and end near present

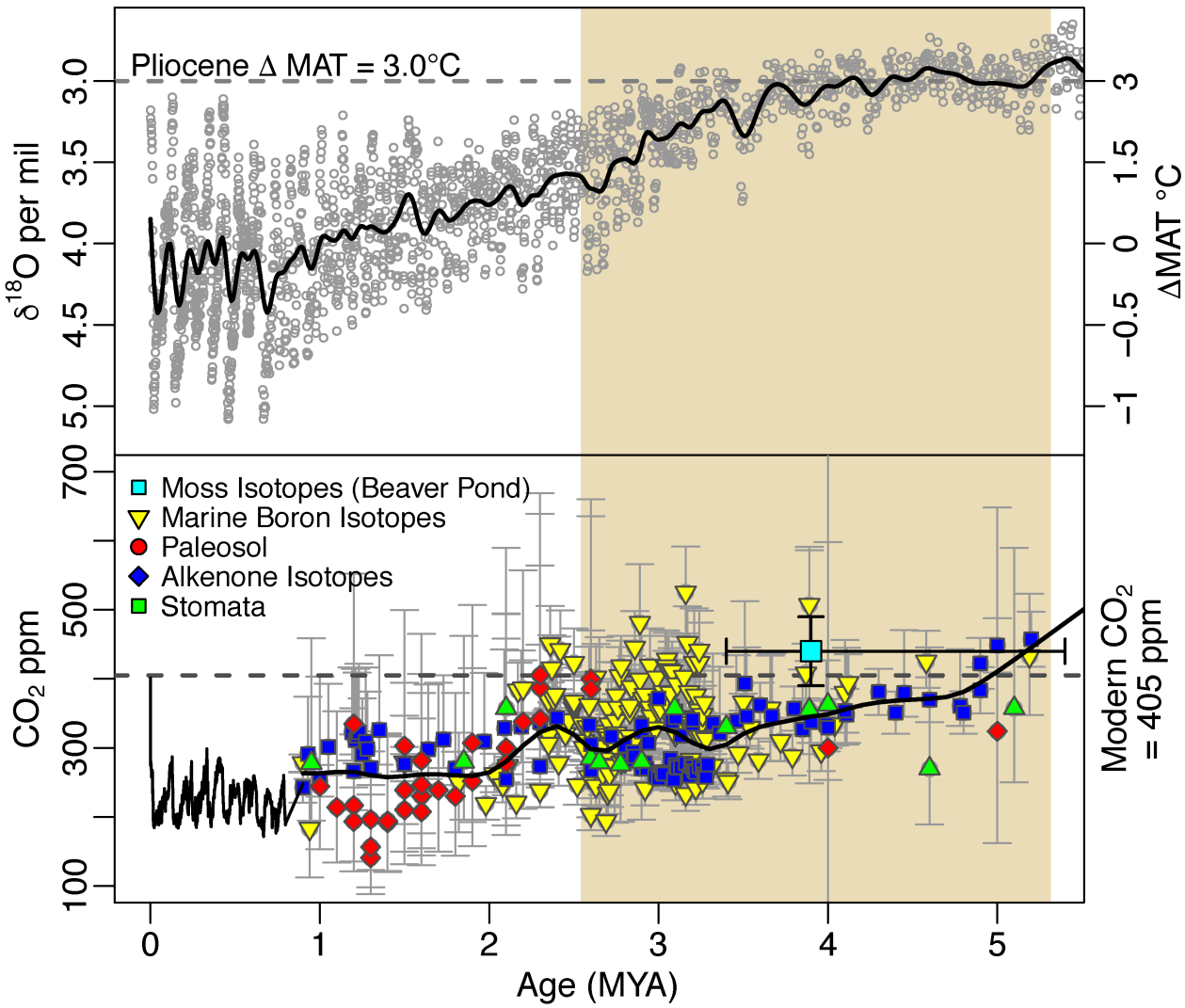

Figure 1: Global temperatures and atmospheric CO_2 concentration spanning the last 5 million years of Earth's history. Mean annual temperatures (MAT) are inferred from compiled $\delta^{18}O$ foraminifera data (Lisiecki and Raymo, 2005) and plotted as anomalies from present (top panel). Modern atmospheric CO_2 measurements (NOAA/ESRL), and ice core observations from EPICA (Luthi et al., 2008) are compared with proxy estimates (bottom panel; see Table S1) for the Pliocene Epoch indicated with beige shading. Smoothed curves have been fit to highlight trends in pCO_2 and temperature during the Pliocene. The results from this paper (BP) are included with both age and pCO_2 error.

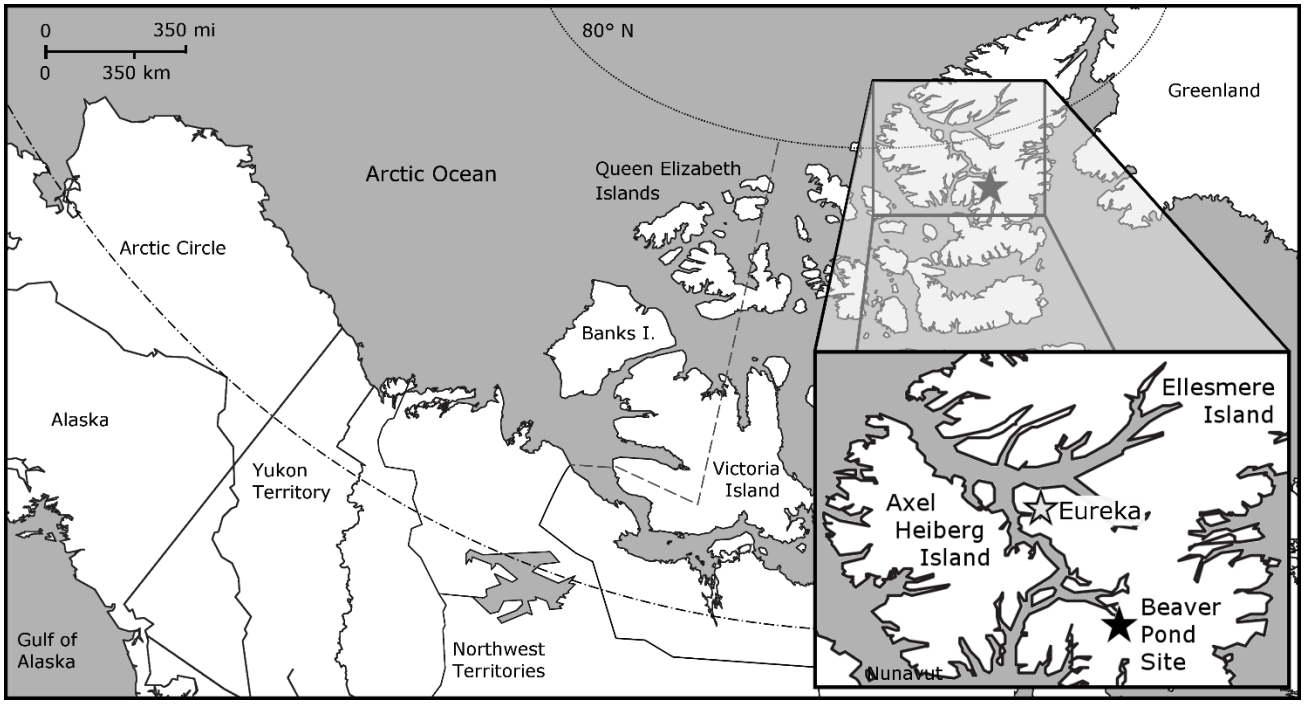

Figure 2. Map of the Canadian Arctic Archipelago, highlighting the location of the Beaver Pond Site (Black Star; 78° 33′ N; 82° 25′ W) and Eureka Climate Station (Grey Star; 80° 13’ N, 86° 11’ W – used for modern climate comparison) on west-central Ellesmere Island.

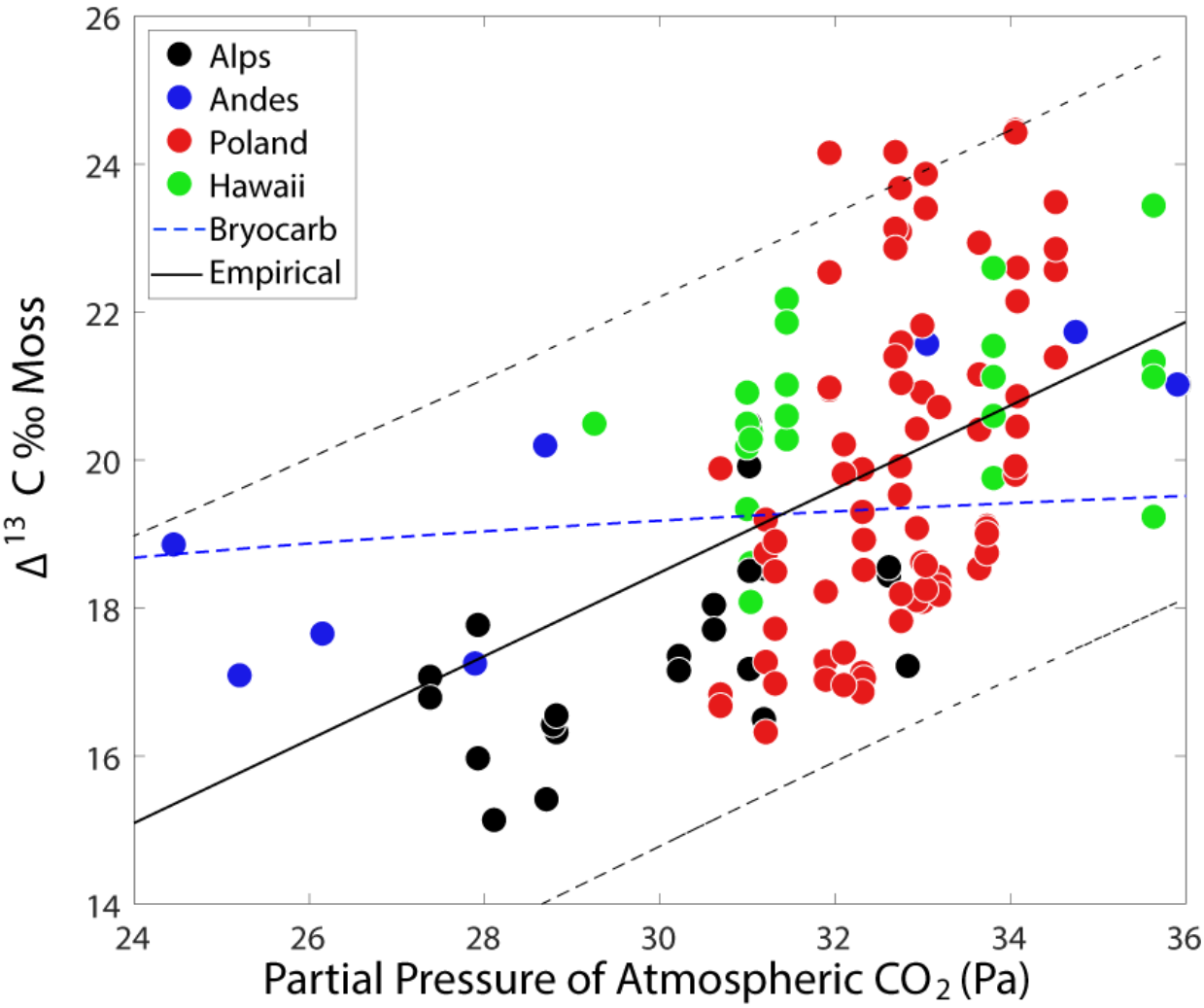

Figure 3. Sensitivity of carbon isotopic discrimination to the partial pressure of atmospheric CO_2 in mosses sampled from different elevational transects. Moss carbon isotope data collected from an elevational transects in the Swiss Alps (black dots; Ménot and Burns, 2001), the Peruvian Andes (blue dots; Royles et al., 2014)), the mountains of Poland (red dots; Skrzypek et al. 2007), and Hawaii (green dots; Waite and Sack 2011). Partial pressure of atmospheric CO_2 calculated from atmospheric surface pressure reanalysis data (Dee et al., 2011) combined with atmospheric CO_2 observations from year moss samples were collected. All carbon isotopic measurements of mosses have been normalized to cellulose based on published regression of cellulose and whole moss values (Ménot and Burns, 2001) and reported as discrimination (Δ) from atmospheric $\delta^{13}CO_2$ (GlobalGlobal View-CO_2, 2013) from the year mosses were collected in units of ‰. Empirical model fit (black line) is plotted with prediction intervals (black dashed) compared with predictions from the BRYOCARB model (blue dashed; Fletcher et al. 2008) with parameters optimized to match observations.

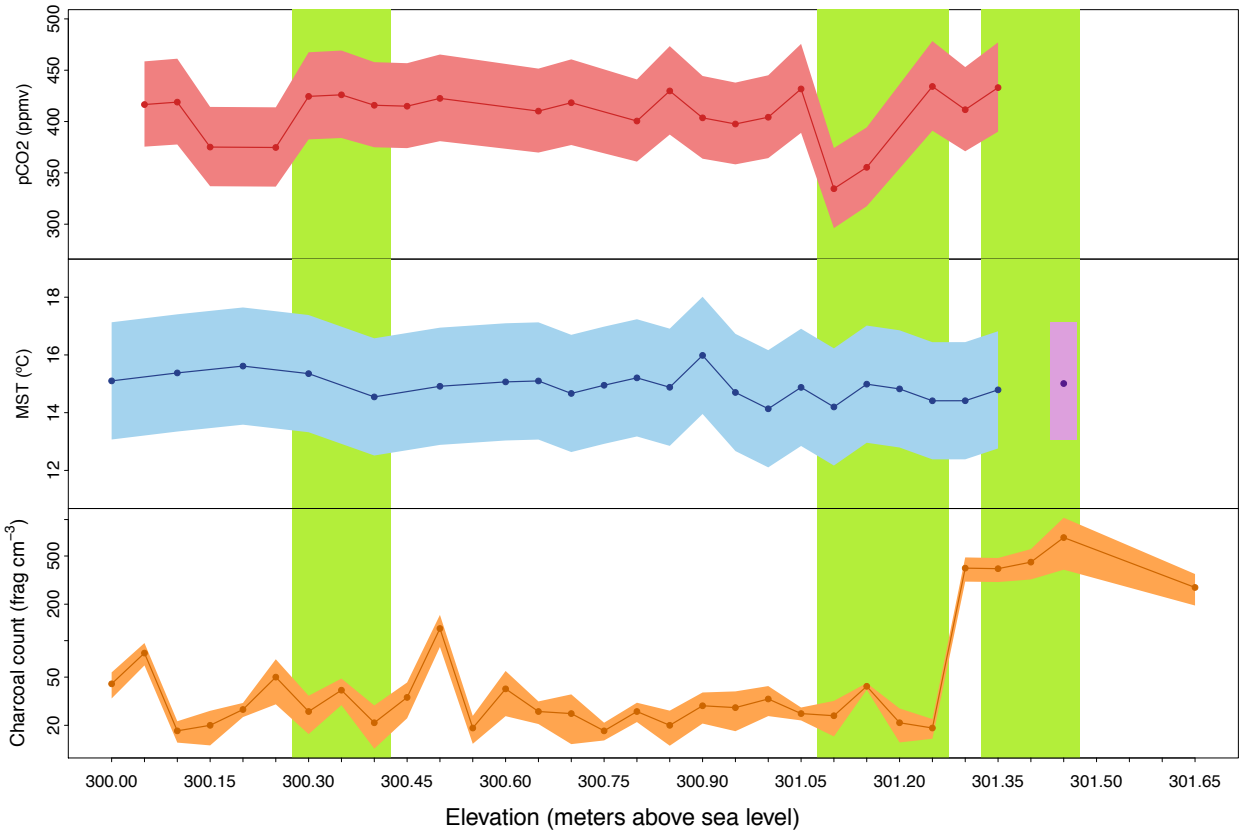

Figure 4. Reconstruction of atmospheric CO_2, mean summer temperature, and fire for the Canadian High Arctic during the Pliocene. Atmospheric CO_2 concentrations estimated from carbon isotopic measurements of mosses and plants (red; ± 2 σ). Mean summer temperature reconstructed from a brGDGT based proxy (blue; ± 2 σ) and relative 2010 data point in approximate relative position (purple; ± 2 σ). Charcoal counts reported as the number of fragments per volume (fragments cm^{-3}) of peat (Orange ± 2 σ). Green boxes indicate relative depths of pollen sampling. Elevation of the deposit is reported as meters above sea level. (Data: Table S3)

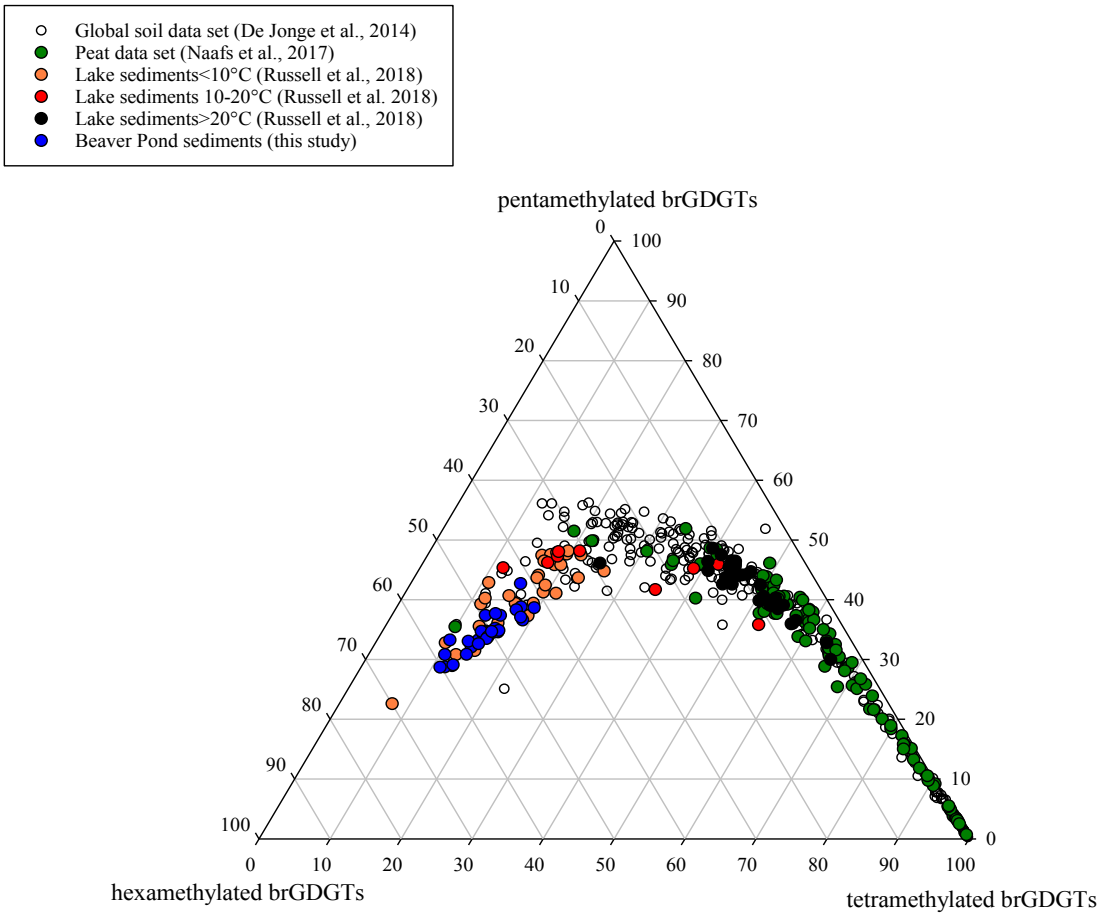

Figure 5. A ternary plot illustrating the fractional abundances of the tetra- (Ia-c), penta (IIa-c and II′a-c), and hexamethylated (IIIa-c and III′a-c) brGDGTs. The global soil dataset (open circles; De Jonge et al., 2014), the global peat samples (green circles; Naafs et al., 2017), and lake sediments from East Africa (black circles indicate samples from lakes >20°C, red circles indicate samples from lakes between 10–20°C and orange circles designate samples from lakes <10°C; Russell et al., 2018) are included for comparison with the Beaver Pond sediments (blue circles; this study).

(A)

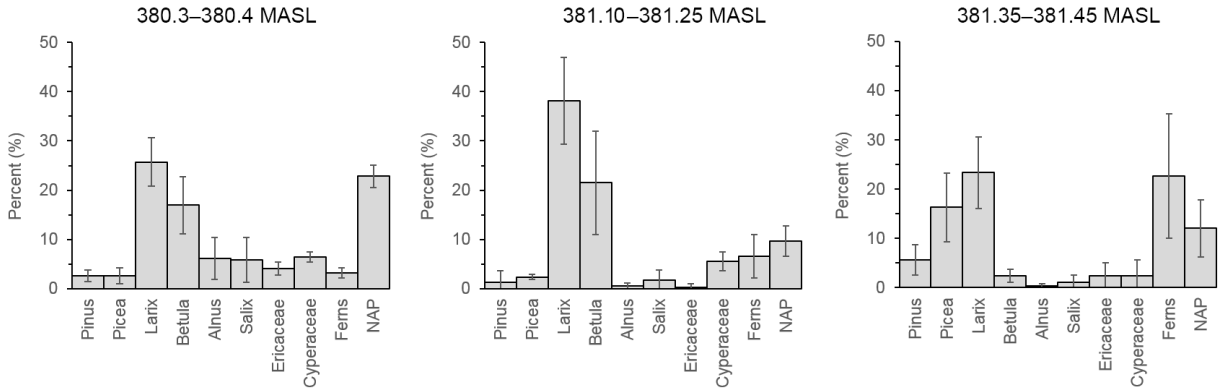

(B)

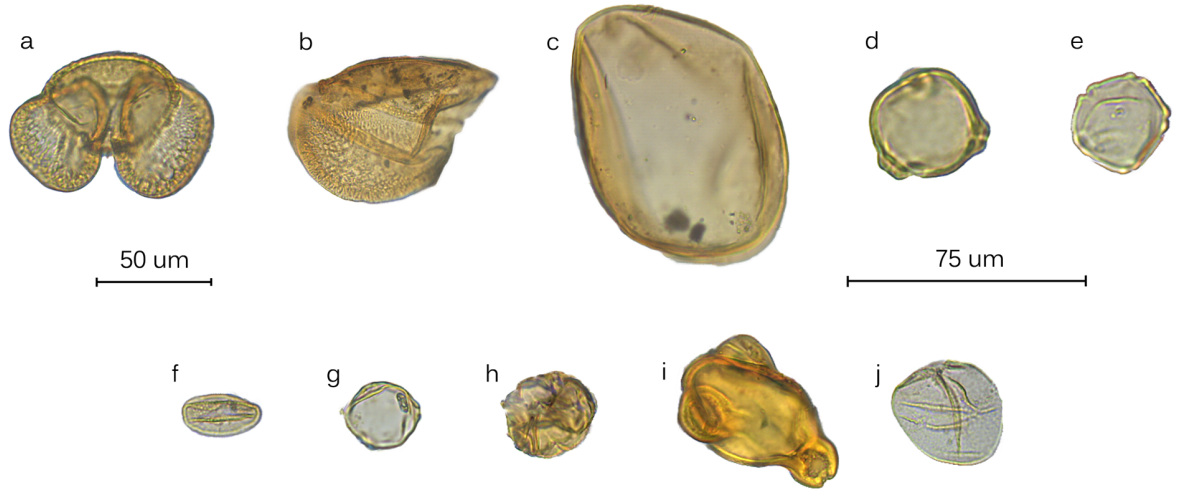

Figure 6. (A) Bar charts showing the relative pollen abundance in each portion of the section (error bars = 95% confidence intervals; MASL- Meters Above Sea Level). (B). Pollen plate of select grains encountered in the BP section: (a) *Pinus*, (b) half a *Picea* grain, (c) *Larix*, (d) *Betula*, (e) *Alnus*, (f) *Salix*, (g) *Myrica*, (h) ericaceous grain, (i) *Epilobium*, and (j) Cyperaceae. 50um scale = (a–c), 75um scale = (d–j).

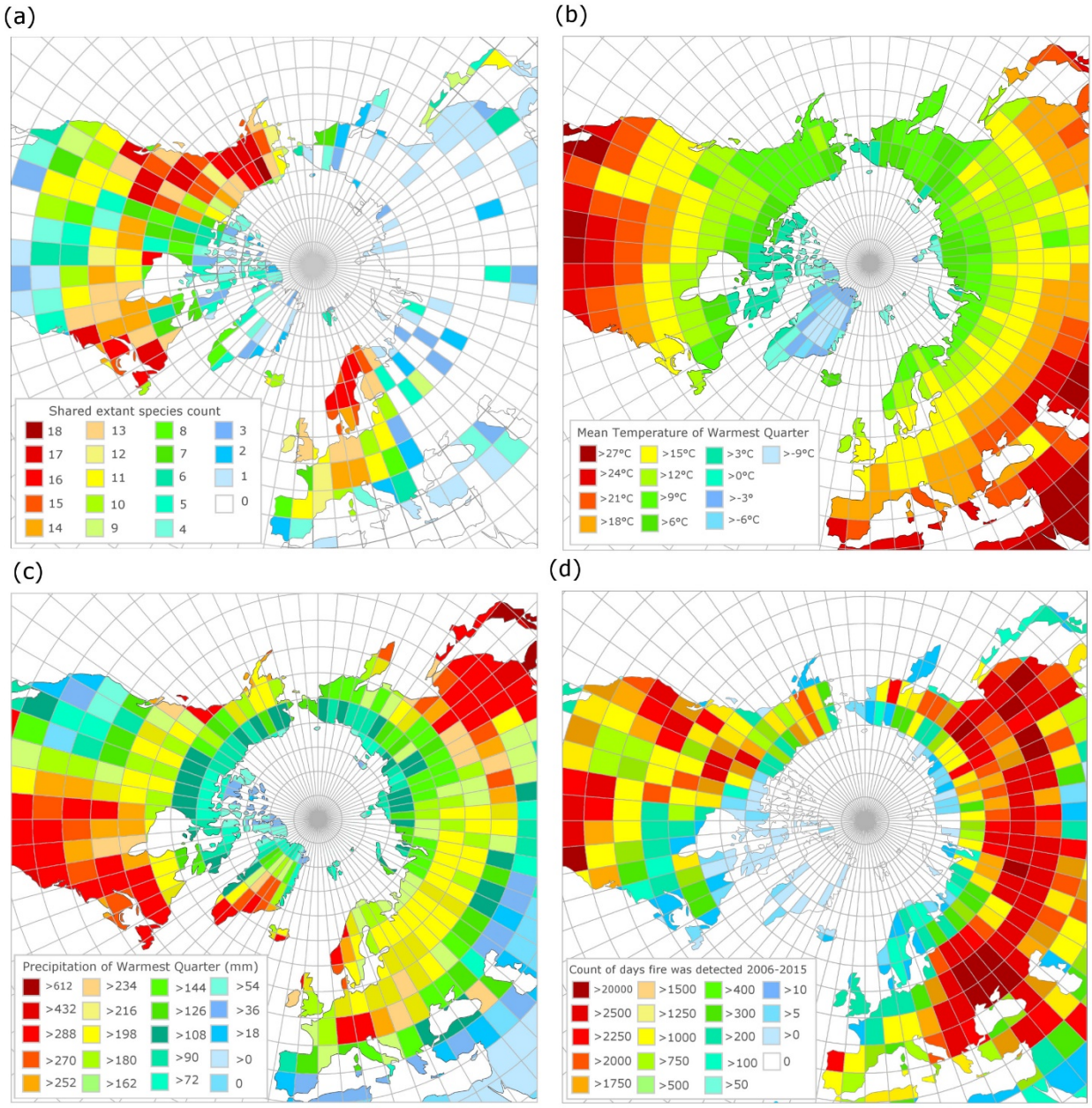

Figure 7. (a) Modern geographic distribution of observed occurrences of species common to the Beaver Pond species list, (b) Mean temperature of the warmest quarter (summer average) derived from WorldClim, (c) Mean precipitation of the warmest quarter (summer rain) derived from WorldClim, (d) Count of unique fire pixels detected per day, over 10 years from MODIS 6 Fire Product, normalized by area of the latitude by longitude grid.